The Institute of Space and Astronautical Science
Report No. 627, March 1988

A Numerical Simulation of Two-Dimensional Transient Shear Flow

By

Yasuhiro KOSHIOKA*

(February, 1988)

Summary: With emphasis on the effect of numerical accuracy of the scheme, a new algorithm is presented on the basis of an improvement of the Arakawa's method, and numerical computation are made for the continuous, transient phenomena of a shear layer from a linear regime to a nonlinear one by use of the Euler equations satisfying vorticity, energy and enstrophy conservations. A comparison is made to clarify the validity of the present scheme applied to the transient phenomena of a shear layer with an assumption of a monochronic disturbance, and detailed examination is made further on the change in flow field of the merging vortices.

Key words: numerical simulation, shear flow, nonlinear instability, transient phenomena

Nomenclatures

$A = \sum_{i',j'} C_{i,j;i',j';i'',j''} \psi_{i+i'',j+j''}$

$B = \sum_{i',j'} C_{i,j;i',j';i'',j''} \zeta_{i+i',j+j'}$

C : Coefficient used in approximation of the Jacobian
D : Deformation tensor
I : Intensity of the Fourier components
i : Unit vector in x-direction
j : Unit vector in y-direction
J : The Jacobian operator
J : The finite difference approximation of the Jacobian
k : Unit vector in z-direction
K : energy of the system
p : Parameter of grid system or nondimensionalized pressure
q : Parameter of grid system
r : Parameter of grid system
v : Velocity vector
V : Enstrophy of the system
x : Coordinate of the physical plane
y : Coordinate of the physical plane
α : Wave number
α_m : Wave number of the maximum growth rate disturbance
κ : Wave number of the system
λ : Wave length
λ_m : Wave length of the maximum growth rate disturbance
ξ : Coordinate of the computational plane
η : Coordinate of the computational plane
ψ : Stream function

* Aircraft Division, Fuji Heavy Industries LTD.

ζ : Vorticity
∇ : $\partial_x i+\partial_y j$
Δ : Grid spacing

Superscripts

$+$: The Jacobian approximation of the first kind
$+*$: The Jacobian approximation of the second kind
$**$: The Jacobian approximation of the third kind
L : The long wave band
M : The medium wave band
S : The short wave band
1 : The approximation to the Jacobian on the referring coordinates
2 : The approximation to the Jacobian on the coordinates obtained by the rotation of the referring coordinates by $\pi/4$
aw : The approximation to the Jacobian on the coordinates obtained by the rotation of the original coordinates by arctan(1/2) anti-clockwise
cw : The approximation to the Jacobian on the coordinates obtained by the rotation of the original coordinates by arctan(1/2) clockwise
o : The approximation to the Jacobian on the original coordinates
′ : small disturbance

1. Introduction

With the development of computers in late '70s and '80s, many direct simulations (in the sense that they do not utilize any assumption or model equation) for shear layers [1, 2] have been carried out using a finite difference scheme.

In general, it is natural that the algorithm of any numerical scheme should be formulated in view of the importance of accuracy of the solutions to the partial differential equations under consideration. However, it must be noted that there seems to exist another viewpoint to be taken into account in making numerical algorithm, that is, the algorithm must satisfy the physical requirements i.e. conservation of vorticity, energy and enstrophy, if any. Of course, if an infinite number of grid points could be utilized to solve the partial differential equations, it would be easily expected that the numerical solution satisfying the physical requirements can be obtained without any difficulty. However, if the simulation is made using a finite number of grid points, it will not be guaranteed that the physical requirements are always satisfied. The reason for adopting Arakawa's method [3] in the present approach may be laid on the fact that it stands upon the latter viewpoint.

As to the total image of the shear layer flow, not only how the transition goes on continuously but also what takes place in the layer are not known precisely yet in the transient process from the linear regime to the fully-developed one. However, it is expected nowadays that the numerical approach may presumably bridge the gap lying between the linear regime of the shear layer and fully developed one, so that the detailed information pertient to the physical process in the transition will be known.

It is the purpose of the present study to demonstrate the importance of satisfying the physical requirements in formulation of an algorithm in order to improve the stability and the accuracy of the solutions in long term numerical integrations. With

emphasis laid on the above-mentioned statement, a modified Arakawa's method is developed for improvement in accuracy and resolution of the numerical solutions, and is applied to clarify the characteristic flow structure of the shear layer in transient process as well as the validity of the above-mentioned concept.

Chapter 2 gives the governing equations. In chapter 3, the numerical algorism used in this study is formulated, in which the modification of Arakawa's method introduced to satisfy the physical requirements is shown. Chapter 4 is devoted to show the results of the present numerical simulations. First of all, simulation with monochronic disturbance under the cyclic boundary condition is carried out for transition from the linear regime to the nonlinear states in order to clarify feasibility of the present numerical algorithm. Then, taking advantage of the results just obtained in the first simulation, some typical processes of vortex-merging are simulated to demonstrate the characteristic flow field. A random disturbance simulation is made in either cyclic boundary condition or flow-out boundary condition in order to demonstrate further the validity of the present scheme. Finally, the concluding remarks are described in chapter 5.

2. Governing equations

In the Cartesian coordinates system (x, y), the Euler equation for incompressible, two-dimensional unsteady flow without external forces can be written using nondimensional expression of the vorticity as

$$\frac{\partial \zeta}{\partial t}+v\cdot \nabla \zeta=0, \tag{2-1}$$

where

$$v=k\times \nabla \psi,$$
$$\zeta=k\cdot \nabla \times v= \nabla^2 \psi,$$

and ψ; the stream function, ∇; the two-dimensional differential operator defined as $\nabla=i\partial_x+j\partial_y$, (i, j); the unit vector in the plane of motion and k; unit vector normal to the plane.

Equation (2–1) can be rewritten as

$$\frac{\partial \zeta}{\partial t}=J(\zeta,\ \psi), \tag{2-2}$$

where J is the Jacobian operator.

3. Numerical algorithm

3–1 General characteristics of numerical scheme

The Jacobian in the governing equation can be replaced by space-differences written in the conventional form such as

$$\mathbf{J}_{i,j}(\zeta,\ \psi)=\frac{1}{4\Delta^2}\{(\zeta_{i+1,\ j}-\zeta_{i-1,j})(\psi_{i,j+1}-\psi_{i,j-1})-(\zeta_{i,j+1}-\zeta_{i,j-1})(\psi_{i+1,j}-\psi_{i-1,j})\}, \tag{3-1}$$

where i and j denote the finite-difference grid indices in x- and y-directions, respectively, and $\triangle$ is the grid spacing. From now on, the bold **J** will denote a finite difference approximation to the Jacobian. If the governing equation is integrated over some hundreds of time steps by use of Eq. (3–1) together with an appropriate time-dependant method with suitable accuracy, it will be easily found that the solution tends to have a characteristic flow structure termed "stretching" or "noodling" [4]. This phenomenon is characterized by the flow structure in which the fluid motion degenerates to eddies that have wave length of a few grid intervals in size and of elongated, filamented shape. In the early stages of this phenomenon, the noodling may be due to the nonlinear effect of governing equation. However, once the noodling is formed, the associated eddies are usually intensified without limit, thus violating numerical solutions to turn out explosive growth of the total kinetic energy of the system. Platzman [4] pointed out the existence of the so-called "aliasing errors," i.e. errors due to misevaluation of the shorter waves, to which the finite grid system is not capable of providing proper resolution (See Appendix A.).

As has been mentioned above, attention must be paid to the following three points in order to carry out numerical simulations adequately, those are alias error, conservation of invariants and phase error (reasonable behavior in convection of physical quantities). There seem to exist two ways to satisfy the second and the third requirements, e. g. the one is to use such a higher-order accuracy scheme as to accomplish conservation of the invariants and low phase error within its accuracy at the same time, and the other is to make first a numerical scheme with the restriction of conservation and then to develop it to higher-order accuracy. Spectral method, pseudospectral method (see Ref. [5]) and modified differential quadrature method (see Ref. [6, 7]) belong to the former, whereas the finite volume method and the Arakawa's method belong to the latter. The former schemes have advantage in the sense of alias free, because they can resolve shorter waves more accurately than the latter, and, above all, the spectral method is perfectly alias free scheme (see Appendix A.). In general, since the latter schemes need a larger number of grid points to identify the same wave number than the former, aliasing to the latter occurs in the earlier stage of computation than the former. Therefore, it is very important to remove the shorter waves that cause the aliasing in any numerical schemes except spectral method.

3–2 Constraints on the advection term

Equation (2–1) implies the conservation of vorticity for individual fluid particles. moreover, since the advection of vorticity as well as any physical quantity in two-dimensional incompressible flow can be expressed by the Jacobian given in Eq. (2–1) or Eq. (2–2), it will be easily known that there are strong integral constraints on the advection term that arises from the nature of the Jacobian. Among these constraints the simplest ones associated with two-dimensional incompressible flow can

be given by the relations

$$\overline{J\ (p,\ q)}=0, \tag{3-2}$$

$$\overline{pJ\ (p,\ q)}=0, \tag{3-3}$$

$$\overline{qJ\ (p,\ q)}=0, \tag{3-4}$$

where p and q are arbitrary arguments and the barred quantities denote the average over the computational domain, along the boundary of which either p or q is constant. From these integral constraints applied to the advection of vorticity, it will be known that the mean vorticity, $\bar{\zeta}$, the mean kinetic energy, $K=\overline{v^2}/2=\overline{(\nabla\psi)^2}/2$, and the mean square vorticity (enstrophy), $V=\overline{\zeta^2}/2=\overline{(\nabla^2\psi)^2}/2$ are conserved with time in a closed domain, having no inflow or outflow across it.

A series expansion of ψ by use of orthogonal harmonic functions, ψ_n, satisfying the equation

$$\nabla^2\psi_n + \kappa_n^2\psi_n=0, \tag{3-5}$$

leads to the following relation for conservation of energy and enstrophy

$$\frac{dK}{dt} = \frac{d}{dt}\sum_n K_n=0, \tag{3-6}$$

$$\frac{dV}{dt} = \frac{d}{dt}\sum_n V_n=0, \tag{3-7}$$

where

$$K_n\equiv\frac{1}{2}\overline{(\nabla\psi_n)^2},$$

$$V_n\equiv\frac{1}{2}\overline{(\nabla^2\psi_n)^2}=\kappa_n^2K_n.$$

Therefore, the average wave number, κ, defined by

$$\kappa^2\equiv\frac{\sum_n \kappa_n^2K_n}{\sum_n K_n}, \tag{3-8}$$

is conserved with time. This implies that no systematic one-way cascade of energy transfer to the shorter waves can occur in two-dimensional incompressible flow, as Fjørtoft [8] pointed out. If three waves (or three groups of waves, each of which has a characteristic average scale) are considered, for example, only the following energy transfer is possible:

$$K_L \leftarrow K_M \rightarrow K_S,$$

or

$$K_L \rightarrow K_M \leftarrow K_S,$$

where K_L, K_M and K_S denote the mean kinetic energies of the long waves, medium waves and short waves, respectively. However, it must be noted that Kraichnan [9] pointed out the occurrence of only the former type of cascades in two-dimensional isotropic turbulence.

3–3 Finite difference approximation of the jacobian

The finite difference expression of the Jacobian at the grid point (i, j) may be written using a relatively general form, as

$$\mathbf{J}_{i,j}(\zeta, \psi) = \sum_{i',j'} \sum_{i'',j''} C_{i,j;i',j';i'',j''} \zeta_{i+i',j+j'} \psi_{i+i'',j+j''}, \tag{3–9}$$

where $\zeta_{i+i',j+j'}$ is the vorticity at a neighboring grid point (i+i', j+j') and $\psi_{i+i'',j+j''}$ is the stream function at a neighboring grid point (i+i'', j+j''). The coefficients $C_{i,j;i',j';i'',j''}$ must be so chosen that Eq. (3–9) becomes an approximation to the Jacobian within the order of necessary accuracy. Moreover, there exist several physical requirements mentioned previously, which must be imposed as constraints on these coefficients.

In order to clarify the condition for conservation of enstrophy, it will be convenient to define

$$A_{i,j;i+i',j+j'} = \sum_{i'',j''} C_{i,j;i',j';i'',j''} \psi_{i+i'',j+j''}. \tag{3–10}$$

It must be noted that $A_{i,j;i+i',j+j'}$ is assumed to be given by a linear combination of the velocity components expressed in finite difference forms of the stream function. Thus, Eq. (3–9) can be reduced to

$$\mathbf{J}_{i,j}(\zeta, \psi) = \sum_{i',j'} A_{i,j;i+i',j+j'} \zeta_{i+i',j+j'}. \tag{3–11}$$

If all of the $\zeta_{i+i',j+j'}$ be formally set equal to a constant, then, Jacobian will vanish regardless of the value of the vorticity. Therefore, the following relation must be held

$$\sum_{i',j'} A_{i,j;i+i',j+j'} = 0, \tag{3–12}$$

which is a finite difference expression for $\nabla \cdot v = 0$, as will be seen later more clearly.

Multiplying Eq. (3–11) by $2\zeta_{i,j}$, then gives

$$2\zeta_{i,j}\mathbf{J}_{i,j}(\zeta, \psi) = \sum_{i',j'} 2\ A_{i,j;i+i',j+j'} \zeta_{i,j} \zeta_{i+i',j+j'} \tag{3–13}$$

It will be found that the left hand side of Eq. (3–13) indicates a temporal change of $\zeta_{i,j}^2$ due to advection. This, in turn, implies that the term $2\ A_{i,j;i+i',j+j'} \zeta_{i,j} \zeta_{i+i',j+j'}$ can be interpreted as the gain of square vorticity at the grid point (i, j) due to the interaction

with the grid point (i+i′, j+j′). Similarly, the term, $2A_{i+i',j+j';i,j}\ \zeta_{i+i',j+j'}\zeta_{i,j}$ can be interpreted as the gain of square vorticity at the grid point (i+i′, j+j′) due to the interaction with the grid point (i, j). In order to avoid false production of square vorticity, these two quantities must have the same magnitude but opposite sign regardless of the values of $\zeta_{i,j}$ and $\zeta_{i+i',j+j'}$. Therefore, the following relations must be held

$$A_{i,j;i+i',j+j'}=-A_{i+i',j+j';i,j}, \tag{3–14}$$

and, in particular,

$$A_{i,j;i,j}=0, \tag{3–15}$$

if the square vorticity is to be conserved in the finite difference scheme.

Replacing i by i−i′ and j by j−j′ in Eq. (3–14) leads to

$$A_{i,j;i-i',j-j'}=-A_{i-i',j-j';i,j}, \tag{3–16}$$

Eqs, (3–11) and (3–12) are now rewritten as

$$\mathbf{J}_{i,j}(\zeta,\ \psi)=\sum_{i',j'}^{*}\{A_{i,j;i+i',j+j'}\zeta_{i+i',j+j'}-A_{i-i',j-j';i,j}\zeta_{i-i',j-j'}\}, \tag{3–17}$$

$$\sum_{i',j'}^{*}\{A_{i,j;i+i',j+j'}-A_{i-i',j-j';i,j}\}=0, \tag{3–18}$$

Where $\sum_{i',j'}^{*}$ denotes summation for the indices $j'>0$, $i'\gtreqless 0$ and $j'=0$, $i'>0$. Taking Eq. (3–18) into account, Eq. (3–17) can also be reexpressed as

$$\mathbf{J}_{i,j}(\zeta,\ \psi)=\sum_{i',j'}^{*}\{A_{i,j;i+i',j+j'}(\zeta_{i+i',j+j'}-\zeta_{i,j})+A_{i-i',j-j';i,j}(\zeta_{i,j}-\zeta_{i-i',j-j'})\}, \tag{3–19}$$

or

$$\mathbf{J}_{i,j}(\zeta,\ \psi)=\sum_{i',j'}^{*}\{A_{i,j;i+i',j+j'}(\zeta_{i+i',j+j'}+\zeta_{i,j})-A_{i-i',j-j';i,j}(\zeta_{i,j}+\zeta_{i-i',j-j'})\}, \tag{3–20}$$

Thus, Eqs. (3–18), (3–19) and (3–20) correspond, respectively, to the differential forms:

$$-\frac{1}{2}\nabla\cdot\mathrm{v}=0, \tag{3–21}$$

$$\mathrm{J}\ (\zeta,\ \psi)=-\mathrm{v}\cdot\nabla\zeta, \tag{3–22}$$

and

$$\mathrm{J}(\zeta,\ \psi)=-\nabla\cdot(\mathrm{v}\zeta). \tag{3–23}$$

The expression given by Eq. (3–19) may be called as "advective form" and the expression given by Eq. (3–20) may be called as "flux form". Both are identical in the non-divergent case. The flux form given by Eq. (3–20) indicates that the flux of a quantity from the grid point (i, j) to the grid point (i+i′, j+j′) can be expressed as a product of the corresponding mass flux and the arithmetic mean of the quantities at the two points.

Multiplying Eq. (3–17) by $2\zeta_{i,j}$, then, gives

$$2\ \zeta_{i,j}\mathbf{J}_{i,j}(\zeta,\ \psi)=\sum_{i',j'}^{*}\{2\ A_{i,j;i+i',j+j'}\zeta_{i,j}\zeta_{i+i',j+j'} -2A_{i-i',j-j';i,j}\zeta_{i,j}\zeta_{i-i',j-j'}\}, \tag{3–24}$$

It is remarkable that the right hand side of Eq. (3–24) again consists of the difference in fluxes of the square vorticity, in which geometrical means appear in contrast with the arithmetic means in Eq. (3–20). Therefore, it is clear that both $\mathbf{J}_{i,j}(\zeta,\ \psi)$ and $2\ \zeta_{i,j}\mathbf{J}_{i,j}(\zeta,\ \psi)$ can be written in flux forms adequately if Eqs. (3–14) and (3–15) are valid.

In the conventional finite difference scheme for the Jacobian, Eq. (3–1), the following relations are used for arbitrary i and j;

$$A_{i,j;i+1,j}=\frac{1}{4\Delta^2}(\psi_{i,j+1}-\psi_{i,j-1}), \tag{3–25}$$

$$A_{i,j;i-1,j}=-\frac{1}{4\Delta^2}(\psi_{i,j+1}-\psi_{i,j-1}), \tag{3–26}$$

$$A_{i,j;i,j+1}=-\frac{1}{4\Delta^2}(\psi_{i+1,j}-\psi_{i-1,j}), \tag{3–27}$$

$$A_{i,j;i,j-1}=\frac{1}{4\Delta^2}(\psi_{i+1,j}-\psi_{i-1,j}), \tag{3–28}$$

Replacing i by i+1 in Eq. (3–26) and j by j+1 in Eq. (3–28), then, leads to

$$A_{i+1,j;i,j}=-\frac{1}{4\Delta^2}(\psi_{i+1,j+1}-\psi_{i+1,j-1}), \tag{3–26′}$$

and

$$A_{i,j+1;i,j}=\frac{1}{4\Delta^2}(\psi_{i+1,j+1}-\psi_{i-1,j+1}). \tag{3–28′}$$

It will be easily known in comparison of Eq. (3–25) with Eq. (3–26′) and Eq. (3–27) with Eq. (3–28′) that Eq. (3–14) is not satisfied by the finite difference scheme given by Eq. (3–1). The net false production of square vorticity that is due obviously to the interactions between the grid points (i, j) and (i+1, j) and also between the grid points (i, j) and (i, j+1) in this scheme can be expressed, respectively, as

$$2(A_{i,j;i+1,j}+A_{i+1,j;i,j})\zeta_{i,j}\zeta_{i+1,j}$$
$$=-\frac{\zeta_{i,j}\zeta_{i+1,j}}{2\Delta^2}\{(\psi_{i+1,j+1}-\psi_{i+1,j-1})-(\psi_{i,j+1}-\psi_{i,j-1})\}, \tag{3-29}$$

and

$$2(A_{i,j;i,j+1}+A_{i,j+1;i,j})\zeta_{i,j}\zeta_{i,j+1}$$
$$=\frac{\zeta_{i,j}\zeta_{i,j+1}}{2\Delta^2}\{(\psi_{i+1,j+1}-\psi_{i+1,j+1})-(\psi_{i+1,j}-\psi_{i-1,j})\}. \tag{3-30}$$

These equations can be further rewritten as

$$\frac{1}{2}(D_{i+1/2,j+1/2}+D_{i+1/2,j-1/2})\zeta_{i,j}\zeta_{i+1,j}, \tag{3-29′}$$

and

$$\frac{-1}{2}(D_{i+1/2,j+1/2}+D_{i-1/2,j+1/2})\zeta_{i,j}\zeta_{i,j+1}, \tag{3-30′}$$

where

$$D_{i+1/2,j+1/2}\equiv\frac{-1}{\Delta^2}(\psi_{i+1,j+1}+\psi_{i,j}-\psi_{i,j+1}-\psi_{i+1,j}).$$

The last expression is a finite difference approximation to the cross derivative $-\partial^2\psi/\partial x\partial y$, which indicates a component of the deformation tensor. Furthermore, the false production of square vorticity, for which $D_{i+1/2,j+1/2}$ is responsible, can be expressed as

$$\frac{1}{2}D_{i+1/2,j+1/2}(\zeta_{i,j}\zeta_{i+1,j}+\zeta_{i,j+1}\zeta_{i+1,j+1}-\zeta_{i,j}\zeta_{i,j+1}-\zeta_{i+1,j}\zeta_{i+1,j+1})$$
$$=\frac{-1}{4}D_{i+1/2,j+1/2}\{(\zeta_{i+1,j}-\zeta_{i,j})^2+(\zeta_{i+1,j+1}-\zeta_{i,j+1})^2-(\zeta_{i,j+1}-\zeta_{i,j})^2-(\zeta_{i+1,j+1}-\zeta_{i+1,j})^2\}.$$

This equation is a finite difference approximation to the quantity

$$\frac{\Delta^2}{2}\frac{\partial^2\psi}{\partial x\partial y}\left\{\left(\frac{\partial\zeta}{\partial x}\right)^2-\left(\frac{\partial\zeta}{\partial y}\right)^2\right\} \tag{3-31}$$

calculated at the point (i+1/2, j+1/2). Whether the total square vorticity in the whole domain increases or decreases depends, therefore, on the sign of the term (3–31).

The general form of the finite difference approximation to the Jacobian at the grid point (i, j), Eq. (3–9) may also be rewritten as

$$J_{i,j}(\zeta,\ \psi)=\sum_{i'',j''}B_{i,j;i+i'',j+j''}\psi_{i+i'',j+j''}, \tag{3-32}$$

where

$$B_{i,j;i+i'',j+j''}=\sum_{i'',j''} C_{i,j;i',j';i'',j''}\zeta_{i+i',j+j'}. \tag{3-33}$$

For quite the same reason as has been already mentioned in Eq. (3-12), the following relation must be valid;

$$\sum_{i'',j''} B_{i,j;i+i'',j+j''}=0. \tag{3-34}$$

Furthermore, corresponding to Eq. (3-14), the integral constraint, $\overline{\psi\ J(\zeta,\ \psi)}=0$, which results in conservation of the kinetic energy in a closed domain, is satisfied by the requirement

$$B_{i,ji+i'',j+j''}=-B_{i+i'',j+j'';i,j}, \tag{3-35}$$

in the finite difference scheme. However, it is evident that the conventional difference scheme given by Eq. (3-1) does not satisfy this requirement and, consequently, it does not conserve kinetic energy.

For simplicity, consider the following four basic second-order finite difference approximations for a square grid, which are given by the following equations:

$$\mathbf{J}^{++}=\frac{1}{4\Delta^2}\{(\zeta_{i+1,j}-\zeta_{i-1,j})(\psi_{i,j+1}-\psi_{i,j-1})-(\zeta_{i,j+1}-\zeta_{i,j-1})(\psi_{i+1,j}-\psi_{i-1,j})\}, \tag{3-36}$$

$$\mathbf{J}^{+*}=\frac{1}{4\Delta^2}\{\zeta_{i+1,j}(\psi_{i+1,j+1}-\psi_{i+1,j-1})-\zeta_{i-1,j}(\psi_{i-1,j+1}-\psi_{i-1,j-1}) -\zeta_{i,j+1}(\psi_{i+1,j+1}-\psi_{i-1,j+1})+\zeta_{i,j-1}(\psi_{i+1,j-1}-\psi_{i-1,j-1})\}, \tag{3-37}$$

$$\mathbf{J}^{*+}=\frac{1}{4\Delta^2}\{\zeta_{i+1,j+1}(\psi_{i,j+1}-\psi_{i+1,j})-\zeta_{i-1,j-1}(\psi_{i-1,j}-\psi_{i,j-1}) -\zeta_{i-1,j+1}(\psi_{i,j+1}-\psi_{i-1,j})+\zeta_{i+1,j-1}(\psi_{i+1,j}-\psi_{i,j-1})\}, \tag{3-38}$$

$$\mathbf{J}^{**}=\frac{1}{8\Delta^2}\{(\zeta_{i+1,j+1}-\zeta_{i-1,j-1})(\psi_{i-1,j+1}-\psi_{i+1,j-1}) -(\zeta_{i-1,j+1}-\zeta_{i+1,j-1})(\psi_{i+1,j+1}-\psi_{i-1,j-1})\}. \tag{3-39}$$

All of these approximations to the Jacobian have not only the integral constraint given by Eq. (3-2) but also the same order of accuracy, as will be seen in the next section. A more general finite difference approximation to the Jacobian may be obtained by a linear combination of these four basic Jacobians. Therefore, it will be reasonable to assume

$$\mathbf{J}_{i,j}(\zeta,\ \psi)=\alpha\,\mathbf{J}_{i,j}^{++}+\beta\,\mathbf{J}_{i,j}^{+*}+\gamma\,\mathbf{J}_{i,j}^{*+}+\delta\,\mathbf{J}_{i,j}^{**}, \tag{3-40}$$

where $\alpha+\beta+\gamma+\delta=1$. Thus, Eq. (3-40) turns out the relations

$$A_{i,j;i+1,j}=\frac{1}{4\Delta^2}\{\alpha(\psi_{i,j+1}-\psi_{i,j-1})+\beta(\psi_{i+1,j+1}-\psi_{i+1,j-1})\}, \tag{3–41.1}$$

$$A_{i,j;i-1,j}=\frac{-1}{4\Delta^2}\{\alpha(\psi_{i,j+1}-\psi_{i,j-1})+\beta(\psi_{i-1,j+1}-\psi_{i-1,j-1})\}, \tag{3–41.2}$$

$$A_{i,j;i,j+1}=\frac{-1}{4\Delta^2}\{\alpha(\psi_{i+1,j}-\psi_{i-1,j})+\beta(\psi_{i+1,j+1}-\psi_{i-1,j+1})\}, \tag{3–41.3}$$

$$A_{i,j;i,j-1}=\frac{1}{4\Delta^2}\{\alpha(\psi_{i+1,j}-\psi_{i-1,j})+\beta(\psi_{i+1,j-1}-\psi_{i-1,j-1})\}, \tag{3–42.4}$$

$$A_{i,j;i+1,j+1}=\frac{1}{4\Delta^2}\{\gamma(\psi_{i,j+1}-\psi_{i+1,j})+\frac{\delta}{2}(\psi_{i-1,j+1}-\psi_{i+1,j-1})\}, \tag{3–41.5}$$

$$A_{i,j;i-1,j-1}=\frac{-1}{4\Delta^2}\{\gamma(\psi_{i-1,j}-\psi_{i,j-1})+\frac{\delta}{2}(\psi_{i-1,j+1}-\psi_{i+1,j-1})\}, \tag{3–41.6}$$

$$A_{i,j;i-1,j+1}=\frac{-1}{4\Delta^2}\{\gamma(\psi_{i,j+1}-\psi_{i-1,j})+\frac{\delta}{2}(\psi_{i+1,j+1}-\psi_{i-1,j-1})\}, \tag{3–41.7}$$

$$A_{i,j;i+1,j-1}=\frac{1}{4\Delta^2}\{\gamma(\psi_{i+1,j}-\psi_{i,j-1})+\frac{\delta}{2}(\psi_{i+1,j+1}-\psi_{i-1,j-1})\}. \tag{3–41.8}$$

Analogously to Eqs. (3–41.2), (3–41.4), (3–41.6), and (3–41.8), the following relations may be obtained

$$A_{i+1,j;i,j}=\frac{-1}{4\Delta^2}\{\alpha(\psi_{i+1,j+1}-\psi_{i+1,j-1})+\beta(\psi_{i,j+1}-\psi_{i,j-1})\}, \tag{3–41.2′}$$

$$A_{i,j+1;i,j}=\frac{1}{4\Delta^2}\{\alpha(\psi_{i+1,j+1}-\psi_{i-1,j+1})+\beta(\psi_{i+1,j}-\psi_{i-1,j})\}, \tag{3–41.4′}$$

$$A_{i+1,j+1;i,j}=\frac{-1}{4\Delta^2}\{\gamma(\psi_{i,j+1}-\psi_{i+1,j})+\frac{\delta}{2}(\psi_{i,j+2}-\psi_{i+2,j})\}, \tag{3–41.6′}$$

$$A_{i-1,j+1;i,j}=\frac{1}{4\Delta^2}\{\gamma(\psi_{i,j+1}-\psi_{i-1,j})+\frac{\delta}{2}(\psi_{i,j+2}-\psi_{i-2,j})\}. \tag{3–41.8′}$$

Comparison of Eq. (3–41.2′) with Eq. (3–41.1), Eq. (3–41.4′) with Eq. (3–41.3), Eq. (3–41.6′) with Eq. (3–41.5) and Eq. (3–41.8′) with Eq. (3–41.7) reveals that the conditions

$$\alpha=\beta,\ \delta=0 \tag{3–42}$$

are necessary to satisfy Eq. (3–16). Thus, the scheme $\alpha(\mathbf{J}_{i,j}^{+,+}+\mathbf{J}_{i,j}^{+,*})+\gamma\mathbf{J}_{i,j}^{*,+}$ together with an additional condition of $2\alpha+\gamma=1$ gives the conservation of square vorticity.

In a similar way, it can be shown that the conditions

$$\alpha=\gamma,\ \delta=0 \tag{3–43}$$

are necessary to satisfy Eq. (3–35) and, consequently, the scheme $\alpha(\mathbf{J}_{i,j}^{+,+}+\mathbf{J}_{i,j}^{*,+})+\beta\mathbf{J}_{i,j}^{+,*}$

with $2\alpha+\beta=1$ confirms the energy conservation.

The consistent choice of the coefficients which satisfy the conservation of both square vorticity and energy simultaneously is given by

$$\alpha=\beta=\gamma=1/3,\ \delta=0. \tag{3-44}$$

This choice determines distinctly the forms of the Jacobian, and it may be easily known that only the linear combination expressed by $(\mathbf{J}^{++}+\mathbf{J}^{+*}+\mathbf{J}^{*+})/3$ will satisfy $J(\zeta,\ \psi)=-J(\psi,\ \zeta)$ and conservation of the quadratic quantitites.

3–4 Accuracy and error isotropy

Since the finite difference approximation for the Jacobian, given by Eq. (3–40) and Eq. (3–44), consists of a linear combination of the basic second-order finite difference schemes given by Eqs. (3–36), (3–37) and (3–38), it may be expected that the approximation has an accuracy of the same order as that of the basic schemes. Expanding ζ and ψ into taylor series around the point (i, j), then, gives

$$\mathbf{J}^{++}=J\ (\zeta,\ \psi)+\frac{\Delta^2}{6}\left\{\frac{\partial\zeta}{\partial x}\frac{\partial^3\psi}{\partial y^3}-\frac{\partial\zeta}{\partial y}\frac{\partial^3\psi}{\partial x^3}+\frac{\partial^3\zeta}{\partial x^3}\frac{\partial\psi}{\partial y}-\frac{\partial^3\zeta}{\partial y^3}\frac{\partial\psi}{\partial x}\right\}+0\ (\Delta^4), \tag{3-45}$$

$$\begin{aligned}\mathbf{J}^{+*}=J\ (\zeta,\ \psi)+\frac{\Delta^2}{6}\Bigg\{&\frac{\partial\zeta}{\partial x}\frac{\partial^3\psi}{\partial y^3}-\frac{\partial\zeta}{\partial y}\frac{\partial^3\psi}{\partial x^3}+\frac{\partial^3\zeta}{\partial x^3}\frac{\partial\psi}{\partial y}-\frac{\partial^3\zeta}{\partial y^3}\frac{\partial\psi}{\partial x}\\&+3\left(\frac{\partial\zeta}{\partial x}\frac{\partial^3\psi}{\partial x^2\partial y}-\frac{\partial\zeta}{\partial y}\frac{\partial^3\psi}{\partial x\partial y^3}\right)+3\left(\frac{\partial^2\zeta}{\partial x^2}-\frac{\partial^2\zeta}{\partial y^2}\right)\frac{\partial^2\psi}{\partial x\partial y}\Bigg\}+0\ (\Delta^4),\end{aligned} \tag{3-46}$$

$$\begin{aligned}\mathbf{J}^{*+}=J\ (\zeta,\ \psi)+\frac{\Delta^2}{6}\Bigg\{&\frac{\partial\zeta}{\partial x}\frac{\partial^3\psi}{\partial y^3}-\frac{\partial\zeta}{\partial y}\frac{\partial^3\psi}{\partial x^3}+\frac{\partial^3\zeta}{\partial x^3}\frac{\partial\psi}{\partial y}-\frac{\partial^3\zeta}{\partial y^3}\frac{\partial\psi}{\partial x}\\&-3\left(\frac{\partial\psi}{\partial x}\frac{\partial^3\zeta}{\partial x^2\partial y}-\frac{\partial\psi}{\partial y}\frac{\partial^3\zeta}{\partial x\partial y^2}\right)-3\left(\frac{\partial^2\psi}{\partial x^2}-\frac{\partial^2\psi}{\partial y^2}\right)\frac{\partial^2\zeta}{\partial x\partial y}\Bigg\}+0\ (\Delta^4),\end{aligned} \tag{3-47}$$

where the subscripts i, j are omitted for simplicity. Since the finite difference approximation to the Jacobian denoted by $\mathbf{J}_1\ (\zeta,\ \psi)$ has been assumed in the present approach as $(\mathbf{J}^{++}+\mathbf{J}^{+*}+\mathbf{J}^{*+})/3$, it can be reduced to

$$\begin{aligned}\mathbf{J}_1=J\ (\zeta,\ \psi)+\frac{\Delta^2}{6}\Bigg\{&\frac{\partial\zeta}{\partial x}\frac{\partial^3\psi}{\partial y^3}-\frac{\partial\zeta}{\partial y}\frac{\partial^3\psi}{\partial x^3}+\frac{\partial^3\zeta}{\partial x^3}\frac{\partial\psi}{\partial y}-\frac{\partial^3\zeta}{\partial y^3}\frac{\partial\psi}{\partial x}\\&+\left(\frac{\partial\zeta}{\partial x}\frac{\partial^3\psi}{\partial x^2\partial y}-\frac{\partial\zeta}{\partial y}\frac{\partial^3\psi}{\partial x\partial y^2}\right)-\left(\frac{\partial\psi}{\partial x}\frac{\partial^3\zeta}{\partial x^2\partial y}-\frac{\partial\psi}{\partial y}\frac{\partial^3\zeta}{\partial x\partial y^2}\right)\\&+\left(\frac{\partial^2\zeta}{\partial x^2}-\frac{\partial^2\zeta}{\partial y^2}\right)\frac{\partial^2\psi}{\partial x\partial y}-\left(\frac{\partial^2\psi}{\partial x^2}-\frac{\partial^2\psi}{\partial y^2}\right)\frac{\partial^2\zeta}{\partial x\partial y}\Bigg\}+0\ (\Delta^4)\\=J\ (\zeta,\ \psi)+\Bigg\{&\frac{\partial(\nabla^2\zeta)}{\partial x}\frac{\partial\psi}{\partial y}-\frac{\partial(\nabla^2\zeta)}{\partial y}\frac{\partial\psi}{\partial x}\end{aligned}$$

$$+\left(\frac{\partial^2\zeta}{\partial x^2}-\frac{\partial^2\zeta}{\partial y^2}\right)\frac{\partial^2\psi}{\partial x\partial y}-\left(\frac{\partial^2\psi}{\partial x^2}-\frac{\partial^2\psi}{\partial y^2}\right)\frac{\partial^2\zeta}{\partial x\partial y}\Big\}+0\ (\Delta^4). \tag{3-48}$$

A simples stream function defined by the equation

$$\psi=-UY+A\ \sin\ (k\ X) \tag{3-49}$$

is introduced to examine the phase error, where (X, Y) are rectangular coordinates obtained by rotation of the original coordinates axes by an angle θ. This is,

$$\left.\begin{aligned} X&=\ x\ \cos\theta+y\ \sin\theta\\ Y&=-x\ \sin\theta+y\ \cos\theta\end{aligned}\right\}\ , \tag{3-50}$$

and the vorticity is given by

$$\zeta=-A\ k^2\ \sin(k\ X). \tag{3-51}$$

The error in the conventional scheme $J^{++}\ (\zeta,\ \psi)$, given by Eq. (3–1), is written as

$$U\ \frac{\partial\zeta}{\partial X}\ \frac{(k\Delta)^2}{6}(\cos^4\theta+\sin^4\theta)+0(\Delta^4). \tag{3-52}$$

In contrast with Eq. (3–52), the error in the scheme $\mathbf{J}_1(\zeta,\ \psi)$, Eq. (3–48), can be expressed as

$$U\ \frac{\partial\zeta}{\partial X}\ \frac{(k\Delta)^2}{6}(\cos^2\theta+\sin^2\theta)^2+0(\Delta^4). \tag{3-53}$$

In the range $0\leqq\theta\leqq\pi/2$, the factor $(\cos^4\theta+\sin^4\theta)$ in Eq. (3–52) has the maximum value equal to 1 at $\theta=0$ and $\theta=\pi/2$ and the minimum value equal to 1/2 at $\theta=\pi/4$. On the other hand, the factor $(\cos^2\theta+\sin^2\theta)^2$ in Eq. (3–53) is always equal to 1, indicating that the orientation error is removed in this case. Therefore, this nature of $\mathbf{J}_1$ is to be called as error isotropy of the second order.

3–5 Extension of Arakawa's method

As orszag et al. [10] pointed out in their simulation of the 2-dimensional isotropic turbulence, Arakawa's method is certainly inferior to the spectral method in the space resolution, and this inferiority becomes more remarkable in case the coarse grid points are used in the calculation. The reason for present improvement of the resolution of Arakawa's method may be laid on this point.

Consider the Jacobian in another coordinates system, which is given in the form

$$J_{X,Y}(\zeta,\ \psi)=\frac{\partial(\zeta,\ \psi)}{\partial(X,\ Y)}=\frac{\partial(\zeta,\ \psi)}{\partial(x,\ y)}\ \frac{\partial(x,\ y)}{\partial(X,\ Y)}. \tag{3-54}$$

If the Jacobian is evaluated in the new grid system obtained through rotation of the original coordinate by $\pi/4$ radian (it has grid spacing of $\sqrt{2}\ \Delta$), and, moreover, if it

is formulated in the same way as $\mathbf{J}_1$ in the original coordinates, the leading term of the phase error in the Jacobian will have the same form as $\mathbf{J}_1$ has in the original coordinates because of its error isotropy of the second order. If the Jacobian is assumed to be given by the equation

$$\mathbf{J}_2(\zeta,\ \psi)=\frac{1}{3}\{\mathbf{J}^{++}_{\pi/4}(\zeta,\ \psi)+\mathbf{J}^{*+}_{\pi/4}(\zeta,\ \psi)+\mathbf{J}^{+*}_{\pi/4}(\zeta,\ \psi)\}, \tag{3–55}$$

where the subscript $\pi/4$ denotes the values in the new coordinates obtained through $\pi/4$ rotation of the original ones in the clockwise, then, all of the total vorticity, the square of vorticity and the energy can also be conserved through the rotation because the origin of the error involved in these constraints consists in the relative position of the points used to evaluated the Jacobian. Since it is obvious that $J^{++}_{\pi/4}(\zeta,\ \psi)$ equals to $J^{**}(\zeta,\ \psi)$ defined by Eq. (3–39) and

$$\begin{aligned}J^{+*}_{\pi/4}=\frac{1}{8\Delta^2}\{&\zeta_{i+2,j}(\psi_{i+1,j+1}-\psi_{i+1,j-1})-\zeta_{i-2,j}(\psi_{i-1,j+1}-\psi_{i-1,j-1})\\&-\zeta_{i,j+2}(\psi_{i+1,j+1}-\psi_{i-1,j+1})+\zeta_{i,j-2}(\psi_{i+1,j-1}-\psi_{i-1,j-1})\},\end{aligned} \tag{3–56}$$

$$\begin{aligned}J^{*+}_{\pi/4}=\frac{1}{8\Delta^2}\{&\zeta_{i+1,j+1}(\psi_{i,j+2}-\psi_{i+2,j})-\zeta_{i-1,j-1}(\psi_{i-2,j}-\psi_{i,j-2})\\&-\zeta_{i-1,j+1}(\psi_{i,j+2}-\psi_{i-2,j})+\zeta_{i+1,j-1}(\psi_{i+2,j}-\psi_{i,j-2})\},\end{aligned} \tag{3–57}$$

the accuracy of $J_2(\zeta,\ \psi)$ can be, therefore, expressed as

$$\begin{aligned}J_2=J(\zeta,\ \psi)+\frac{\Delta^2}{3}\Big\{&\frac{\partial\zeta}{\partial x}\frac{\partial^3\psi}{\partial y^3}-\frac{\partial\zeta}{\partial y}\frac{\partial^3\psi}{\partial x^3}+\frac{\partial^3\zeta}{\partial x^3}\frac{\partial\psi}{\partial y}-\frac{\partial^3\zeta}{\partial y^3}\frac{\partial\psi}{\partial x}\\&+\Big(\frac{\partial\zeta}{\partial x}\frac{\partial^3\psi}{\partial x^2\partial y}-\frac{\partial\zeta}{\partial y}\frac{\partial^3\psi}{\partial x\partial y^2}\Big)-\Big(\frac{\partial\psi}{\partial x}\frac{\partial^3\zeta}{\partial x^2\partial y}-\frac{\partial\psi}{\partial y}\frac{\partial^3\zeta}{\partial x\partial y^2}\Big)\\&+\Big(\frac{\partial^2\zeta}{\partial x^2}-\frac{\partial^2\zeta}{\partial y^2}\Big)\frac{\partial^2\psi}{\partial x\partial y}-\Big(\frac{\partial^2\psi}{\partial x^2}-\frac{\partial^2\psi}{\partial y^2}\Big)\frac{\partial^2\zeta}{\partial x\partial y}\Big\}+0(\Delta^4).\end{aligned} \tag{3–58}$$

From Eqs. (3–48) and (3–58) it will be easily found that $2J_1(\zeta,\ \psi)-J_2(\zeta,\ \psi)$ is a fourth order approximation of the Jacobian; that is,

$$2\mathbf{J}_1(\zeta,\ \psi)-\mathbf{J}_2(\zeta,\ \psi)=J(\zeta,\ \psi)+0(\Delta^4). \tag{3–59}$$

However, this Jacobian does not have the fourth-order error isotropy, which will be shown in the later arguments.

It must be noted that it is necessary to estimate several higher-order cross-derivatives in order to get the Jacobian having the error isotropy of the fourth-order. For this purpose it will be convenient to introduce the two other coordinates that can be obtained through rotation of the original coordinates by $\arctan(1/2)$ in the clockwise and in the anti-clockwise (they have grid spacing of $\sqrt{5}\,\Delta$), respectively, and the evaluation of the Jacobian in these coordinates can be made in the similar way (the components of these finite difference approximation of Jacobians are shown in

Appendix B.). The phase error involved in the scheme $\mathbf{J}_O=2\mathbf{J}_{1O}-\mathbf{J}_{2O}$ is given as

$$U\frac{\partial\zeta}{\partial X}\frac{(k\Delta)^4}{30}(-\cos^6\theta-\sin^6\theta)+0(\Delta^6), \tag{3-60}$$

where subscript O denotes the values in the original coordinates. The error involved in the scheme, $\mathbf{J}_{CW}=2\mathbf{J}_{1CW}-\mathbf{J}_{2CW}$, may be written as

$$U\frac{\partial\zeta}{\partial X}\frac{(k\Delta)^4}{30}\{-13(\cos^6\theta+\sin^6\theta)+36(\cos^4\theta-\sin^4\theta)\cos\theta\sin\theta$$
$$-60(\cos^2\theta+\sin^2\theta)\cos^2\theta sin^2\theta\}+0(\Delta^6), \tag{3-61}$$

where subscript cw denotes the values in the new coordinates obtained through rotation of the original coordinates in the clockwise by arctan(1/2). The error involved in the scheme, $\mathbf{J}_{AW}=2\mathbf{J}_{1AW}-\mathbf{J}_{2AW}$, may be expressed as

$$U\frac{\partial\zeta}{\partial X}\frac{(k\Delta)^4}{30}\{-13(\cos^6\theta+\sin^6\theta)-36(\cos^4\theta-\sin^4\theta)\cos\theta\sin\theta$$
$$-60(\cos^2\theta+\sin^2\theta)\cos^2\theta sin^2\theta\}+0(\Delta^6), \tag{3-62}$$

where subscript aw denotes the values in the new coordinates obtained through anti-clockwise rotation of the original coordinates by arctan(1/2). Thus, in view of Eqs. (3-60), (3-61) and (3-62), the finite difference approximation of the Jacobian with error isotropy of the forth-order can be formulated as;

$$\mathbf{J}(\zeta,\ \psi)=(14\mathbf{J}_0+\mathbf{J}_{CW}+\mathbf{J}_{AC})/16, \tag{3-63}$$

and the phase error may be reduced to

$$U\frac{\partial\zeta}{\partial X}\frac{(k\Delta)^4}{12}\{-(\cos^6\theta+\sin^6\theta)-3(\cos^2\theta+\sin^2\theta)\cos^2\theta\sin^2\theta\}+0(\Delta^6)$$
$$=U\frac{\partial\zeta}{\partial X}\frac{(k\Delta)^4}{12}\{-(\cos^2\theta+\sin^2\theta)^3\}+0(\Delta^6). \tag{3-64}$$

In the same way, the 6th-order scheme with error isotropy will be obtained by use of 54 basic finite difference approximations of the Jacobian.

A comparison of the resolution between the conventional Arakawa's method and the present one is made in the case of the same intensity merging (see 4-3) and the result is shown in Fig. 1. In the present result, there can be seen a remarkable improvement in resolution of the flow field. The numerical results obtained by use of the conventional scheme having no error isotropy are also compared with the ones obtained by the present method. In Fig. 3, it is obvious that the vortex sheet gradually loses its regularity in the result obtained by Kawamura's method, whereas it is still regular in the result obtained by the present method, as is seen in Fig. 2.

3-6 The method for prevention of alias error

As has been already pointed out by Orszag et al. (see Appendix A.), aliasing occurs if there exist disturbances having the maximum wavenumber that can be resolved by

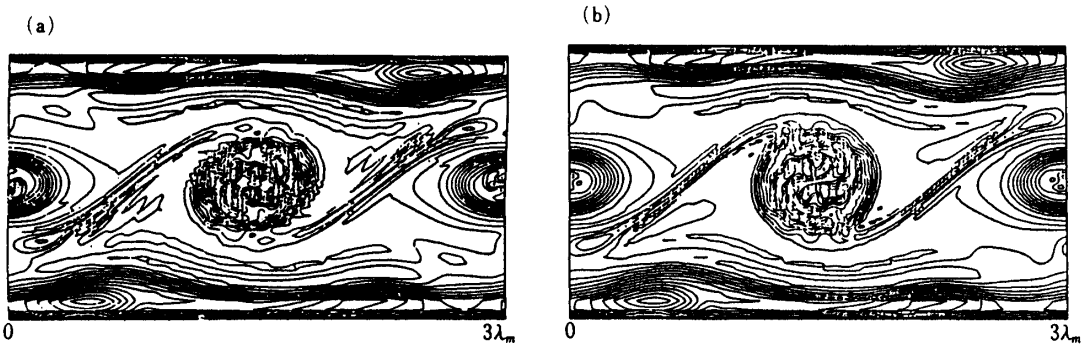

Fig. 1. Vorticity contours of merging vortices in the case of same intensity merging at t=140.
(a) conventional Arakawa's method
(b) present method.

discrete points. Moreover, in case a finite difference scheme is used to simulate nonlinear phenomenon, aliasing also occurs before the disturbance reaches the maximum wave number, because the resolution of the finite idfference scheme is not accurate enough in the region near the maximum wave number (comparison between either the second or the fourth-order finite difference scheme and the Fourier analysis in a linear problem reveals that the former group requires typically 8 to 20 points per wavelength depending on the order of the accuracy of the finite difference scheme, whereas the latter requires only 2 points [11, 12]). Because of this, it is necessary to keep the energy contained in the region near the maximum wave number small enough to avoid the aliasing. Physically speaking, this implies that an energy sink must be set up in this wave number range (see Ref. [13]). If there is no energy sink in the higher range of wave number, the flow pattern will be enveloped with fine wrinkles (see Fig. 4).

It must be noted that, in the present study, the diffusion terms of the 8th- and 6th-orders are employed as energy sinks. The reason for this may be laid on the following statements. The higher diffusion term suppresses disturbance components of very high wave number, so that there remains very weak oscillation in the middle wave number range. This can be interpreted into that the 8th-order diffusion plays a main role as an energy sink, whereas the 6th-order diffusion attenuates such a very weak oscillation that the 8th-order cannot remove. The coefficients of these terms are determined empirically, those are, -10^{-4} for the 6th-order diffusion and 10^{-2} for the 8th-order one. Detailed discussion on the foregoing procedure should be referred to Appendix D.

3–7 Finite difference approximation of the Jacobian and Poison equation in general coordinates

In view of Eq. (3–44), the finite difference approximation of the Jacobian in general coordinates can be expressed as

$$J_{x,y}(\zeta,\ \psi)=\frac{\partial(\zeta,\ \psi)}{\partial(x,y)}=\frac{\partial(\zeta,\ \psi)}{\partial(\xi,\eta)}\frac{\partial(\xi,\ \eta)}{\partial(x,y)}$$
$$=J_{\xi,\eta}(\zeta,\ \psi)\ (\xi_x\eta_y-\xi_y\eta_x), \tag{3–65}$$

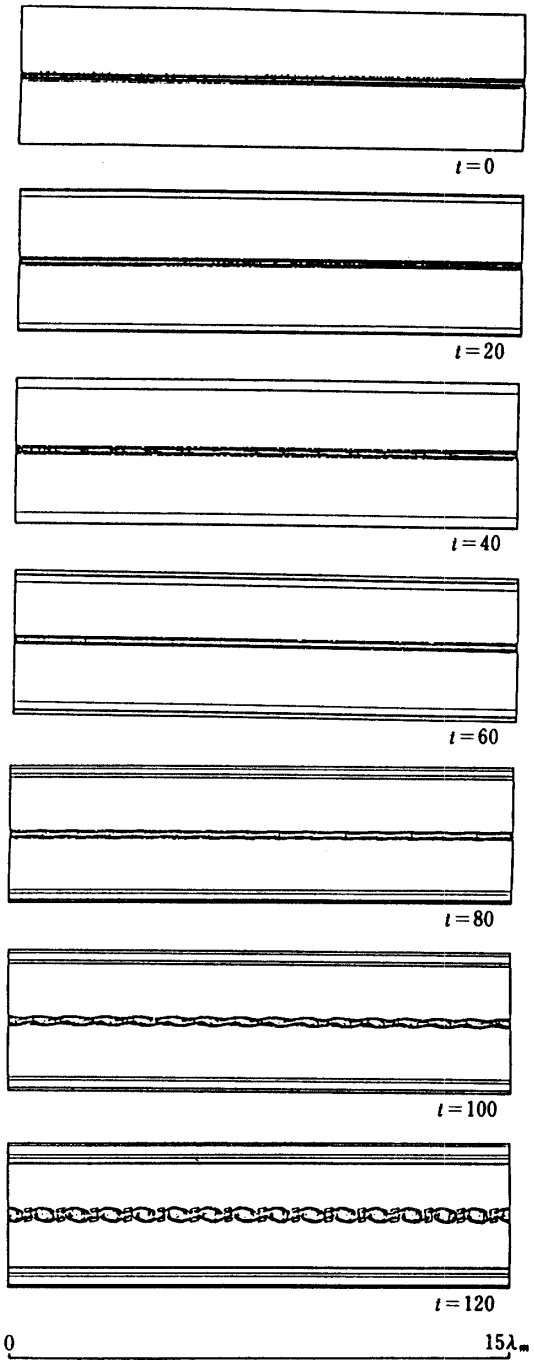

Fig. 2. Temporal evolution of the vorticity contours on the coarse grid system with step 0.04 obtained by the present method from t=0 to 120 (continued). (monochronic initial disturbance and cyclic boundary condition are adopted)

where ξ, η are the Cartesian coordinates in the computational plane. The left hand side of Poison equation for the stream function can be written in the general coordinates as

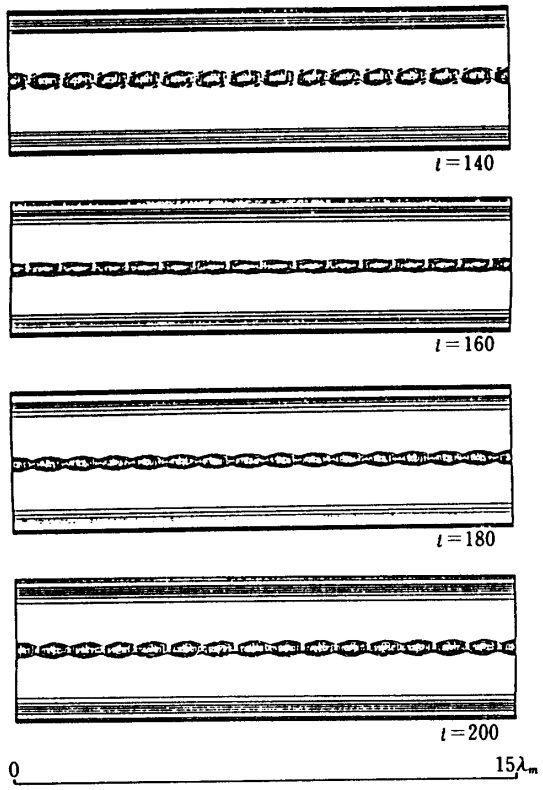

Fig. 2. Temporal evolution of the vorticity contours on the coarse grid system with step 0.04 obtained by the present method from t=140 to 200.
(monochronic initial disturbance and cyclic boundary condition are adopted)

$$\nabla^2_{x,y}\psi=\alpha\psi_{\xi\xi}+2\beta\psi_{\xi\eta}+\gamma\psi_{\eta\eta}+\sigma\psi_{\xi}+\tau\psi_{\eta}, \tag{3-66}$$

where

$$\alpha=\xi_x^2+\xi_y^2,\ \beta=\xi_x\eta_x+\xi_y\eta_y,\ \gamma=\eta_x^2+\eta_y^2,$$
$$\sigma=\xi_{xx}+\xi_{yy},\ \tau=\eta_{xx}+\eta_{yy}.$$

Since the stream function ψ is obtained by integrating vorticity distribution in the computational domain, the resolution that is necessary for calculating the stream function is not so serious as vorticity convection equation. For this reason, the three points conventional finite difference approximations are utilized in Eq. (3–66), and $\nabla^2\zeta$ is given in the same way as Eq. (3–66).

3–8 Time integration

Lilly [14] used Arakawa's method in his numerical simulation of 2-dimensional isotropic turbulence, in which the second-order Adames-Bashforce scheme was employed in integrating Eq. (2–1). The results of the calculation indicate that, if the Courant number is small enough (about 0.2), the accuracy of the first-order time

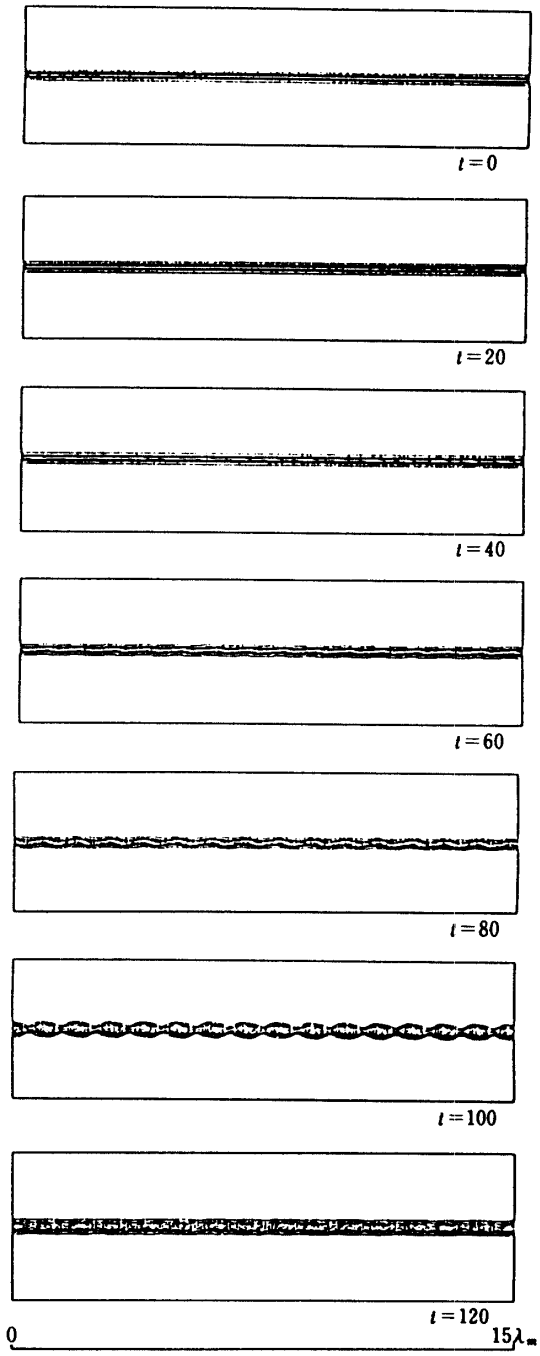

Fig. 3. Temporal evolution of the vorticity contours with step 0.04 obtained by Kawamura's method from t=0 to 120 (continued).
(monochronic initial disturbance and cyclic boundary condition are adopted)

integration seems to be satisfactory in view of the comparison of the growth rate between linear theory and the numerical simulation. Therefore, the first-order time integration is adopted in the present study.

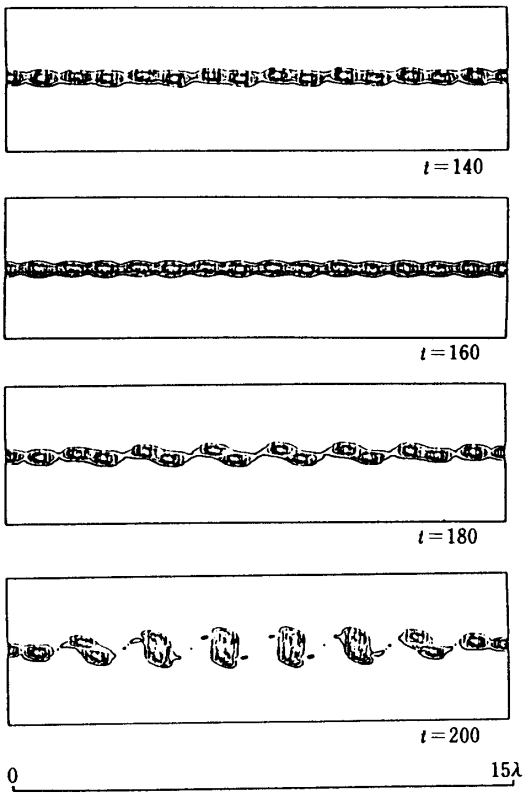

Fig. 3. Temporal evolution of the vorticity contours on the coarse grid system with step 0.04 obtained by Kawamura's method from t=140 to 200.
(monochronic initial disturbance and cyclic boundary condition are adopted)

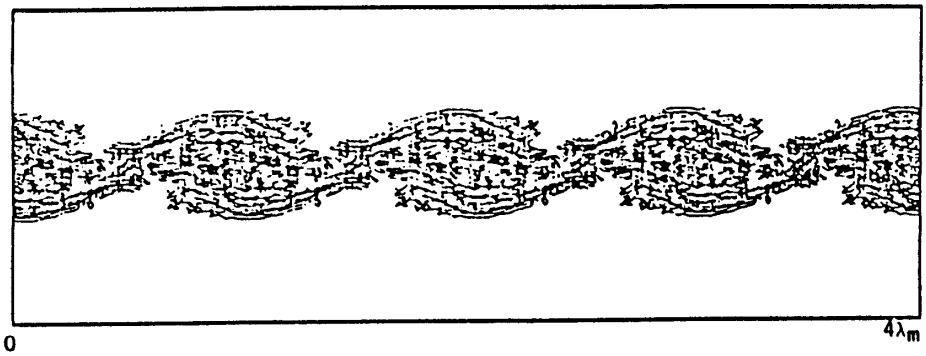

Fig. 4. Vorticity contours of the simulation with aliasing obtained by the present method.
(monochronic initial disturbance and cyclic boundary condition are adopted)

4. Numerical simulations

4–1 Assumptions and grid system

The typical behavior of the shear layer clearly results from the nonlinearity of the governing equation, whereas the viscosity mainly affects the short waves caused by

nonlinear effects. For this reason, it will be reasonable in this study to assume that the diffusion coefficient is negligible and, consequently, the simulations may presumably be made satisfactorily by solving Euler equation numerically. The hyperbolic-tangent velocity profile is particularly adopted to compare the present results on growth rate and vortex contour in the linear regime with those obtained by Michalke [15].

The grid system utilized in the present computation is generated by the equation;

$$\left.\begin{aligned} x&=p\ \xi \\ y&=q\ \eta^3+r\eta \end{aligned}\right\}, \tag{4–1}$$

where the constants p, q, r and the number of utilized grid points are chosen adequately in each simulation.

4–2 Simulation with monochronic disturbance

First of all, consider the shear layer generated by two uniform flows having the same speed but opposite direction, where a hyperbolic-tangent velocity profile (see Fig. 5(a)) is assumed for simplicity. The grid system used in this simulation is 128×65 ($0 \leqq \xi \leqq 127$, $-32 \leqq \eta \leqq 32$) and the coefficients in Eq. (4–1) are $p=(2\pi/\alpha)\ (3/128)$, $q=.1248$ and $r=.0002$, where α denotes the wavenumber of the initial disturbance. The time increment Δ_t was taken to be .025 and the Courant number was preserved less than .2 throughout the computation. The slab symmetry condition was imposed on the upper and lower boundaries and the cyclic boundary condition was imposed on the inflow and out flow boundaries.

The initial conditions were given as follows;

$$\psi=\psi_0+(A/\alpha)\cos(\alpha x)\exp(-\alpha y^2), \tag{4–2–1}$$

$$\zeta=\zeta_0+\alpha A(4y^2-1)\cos(\alpha x)\exp(-\alpha y^2), \tag{4–2–2}$$

where

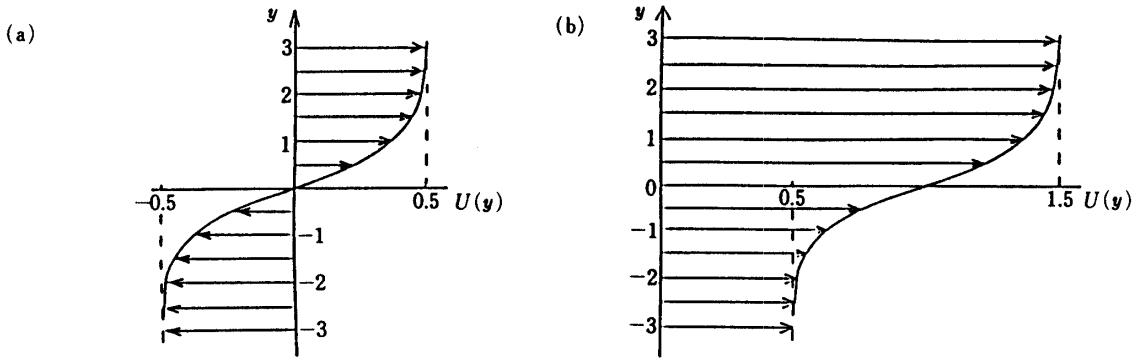

Fig. 5. Sketches of the velocity profile
(a) used in cyclic boundary condition case
(b) used in flow out boundary condition case.

$$\psi_0 = -\log(\cosh(y))/2,$$

$$\zeta_0 = -\mathrm{sech}^2(y)/2,$$

and where A is the amplitude coefficient equal to 10^{-6} and α is the wavenumber of the disturbance.

In Fig. 6, the growth rate of ψ' in the linear regime is plotted for three wavenumbers α_m, $(4/5)\alpha_m$ and $(6/5)\alpha_m$, where $\alpha_m = .4446$ indicates the wavenumber for the maximum growth rate that can be expected from the calculation of Mickalke [15]. It must be noted that the growth rate obtained by the present computation agrees quite well with the one calculated by small disturbance theory (see Fig. 6, 7). Since the cyclic boundary condition has a trend to suppress the generation of high wavenumber disturbance and, consequently, the nonlinear effect is decayed, the linear region is kept to the the disturbance intensity of the order of 10^{-1}. Fig. 8 (t=60 to 80) show the vorticity contours at several early stage of the present simulation, indicating that the results agree qualitatively with those obtained by Michalket [15] (see Fig. 9).

Examination of validity of the present simulation in the later stage can be made in comparison between the numerical results of asymptotic behavior of the vortex roll ups obtained by vortex method by Kransny [16] and those obtained by the present method. Fig. 8 (t=120 to 180) and Fig. 10 indicate qualitatively good agreement in the roll-up pettern of vortex sheet.

From these results, it may be concluded that the present algorithm can predict the transient process of the shear layer more accurately than the existing scheme, if realistic boundary condition is prescribed.

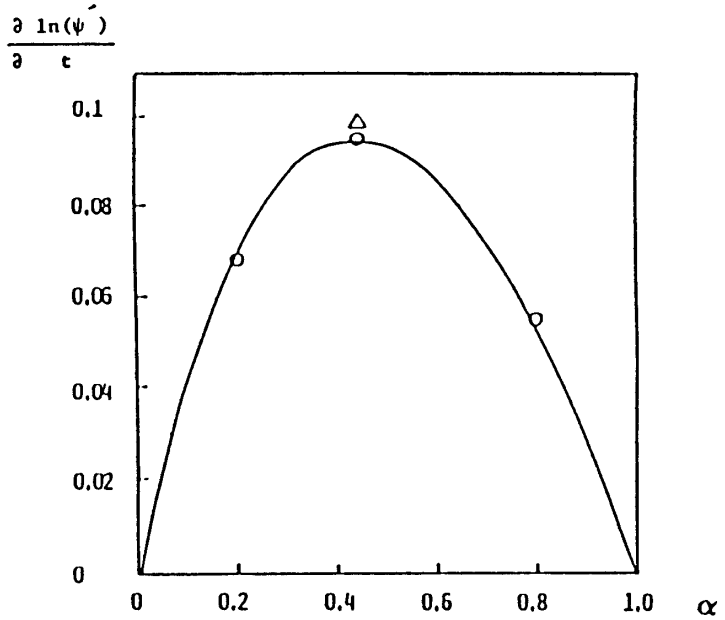

Fig. 6. Linear growth rate us. wavenumber.
—: Small disturbance theory, ○: present method, △: Kawamura's method.

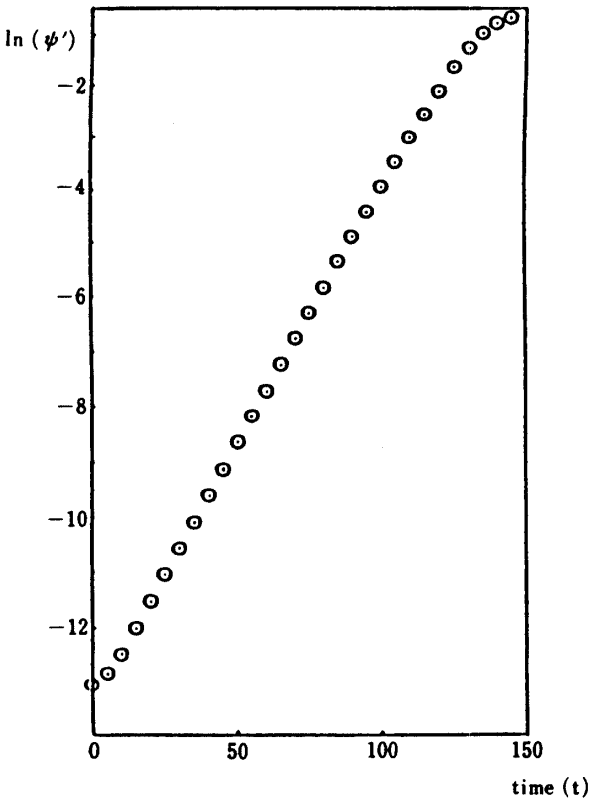

Fig. 7. Typical temporal evolution of the amplitude of the disturbance to the stream function in the linear regime (α=0.4446).

4–3 Simulation of typical merging process

It will be easily known from the foregoing statement that the vortex generated by the shear layer can be controlled without difficulty by the initial disturbance. From this viewpoint, two typical types of merging process of vortices are to be considered, i.e. the merging of the vortices having the same magnitude of vorticity and the merging of the vortices having different magnitude of vorticity. It must be noted that the same computational conditions are used for simulations to the former.

The computation for the first merging process was carried out with the assumption that the initial disturbance involved in the flow field is given by the equation

$$\psi=\psi_0+(A/\alpha_m)\cos(\alpha_1 x)\exp(-\alpha_m y^2) +(A/\alpha_m)\cos(\alpha_2 x)\exp(-\alpha_m y^2), \tag{4–3–1}$$

$$\zeta=\zeta_0+(A/\alpha_m)(4\alpha_m^2 y^2-\alpha_1^2)\cos(\alpha_1 x)\exp(-\alpha_m y^2) +(A/\alpha_m)(4\alpha_m^2 y^2-\alpha_2^2)\cos(\alpha_2 x)\exp(-\alpha_m y^2), \tag{4–3–2}$$

where ψ_0 and ζ_0 are the same as in Eqs. (4–2), and where $\alpha_1=(4/5)\alpha_m$ and $\alpha_2=(6/5)\alpha_m$. The coefficients of grid system were taken to be $p=(2\pi/\alpha_m)(5/6)(3/128)$,

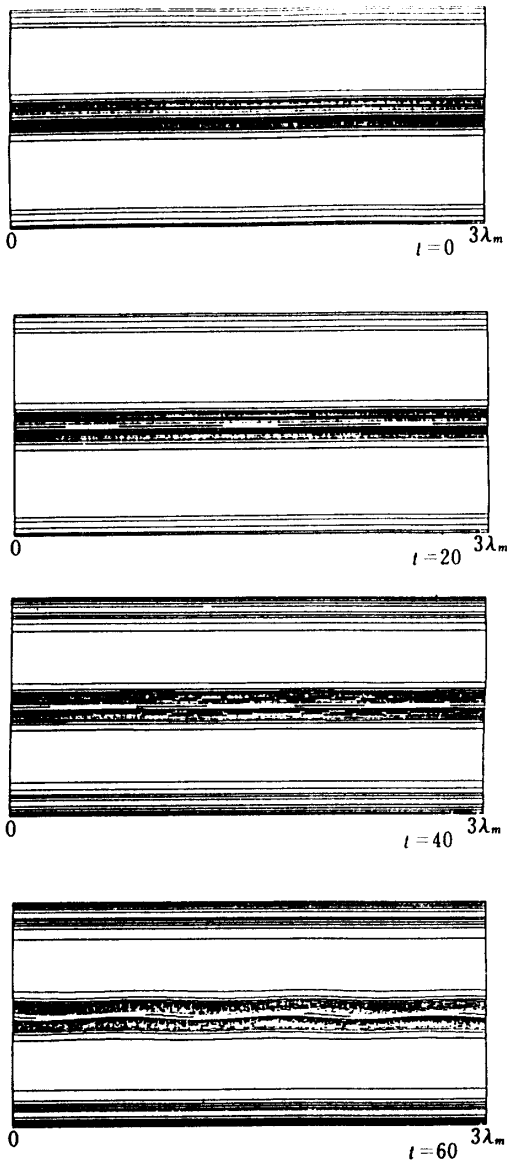

Fig. 8. Temporal evolution of the vorticity contours obtained by the present method with step 0.04 from t=0 to 60 (continued).
(monochronic initial disturbance and cyclic boundary condition are adopted)

q=.1248 and r=.0002, and the same number of grid points were used as the former simulation.

Fig. 11 shows that, at an early stage of the time, three roll-ups of vortex sheet make their appearance in the shear layer, and, meanwhile, the Fourier analysis applied in the x-direction reveals the existence of the components originated from the nonlinear interaction between α_1 and α_2. With the time elapsed these components enhance the trend to merge neighboring vortices of the same intensity. Moreover, it can be observed obviously in the inner structure of the merged vortex that the small scale vortices resulting from the merging process are gradually integrated into larger ones.

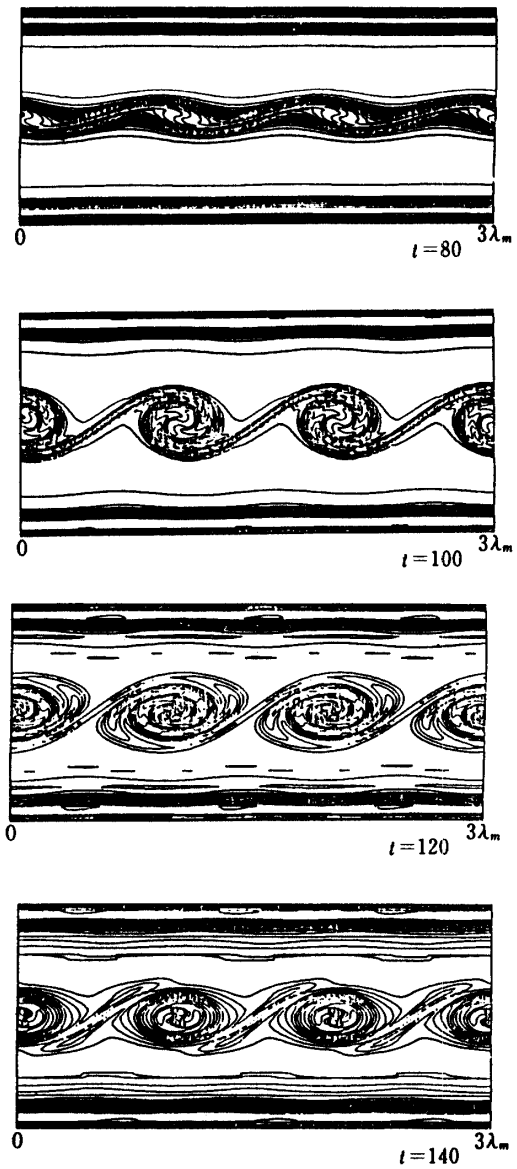

Fig. 8. Temporal evolution of the vorticity contours obtained by the presemt method with step 0.04 from t=80 to 140 (continued).
(monochronic initial disturbance and cyclic boundary condition are adopted)

On the other hand, the vortex intensified by the merging process tears the vortex sheet to spread the shear layer. From now on, the merging process of this kind is called as "the same intensity merging."

The other one can be simulated with the initial condition given by Eqs. (4–3), where $\alpha_1=(3/2)\alpha_m$, $\alpha_2=(3/4)\alpha_m$ and the amplitude $A=10^{-4}$ have been employed. The coefficients of grid system were set to be $p=(2\pi/\alpha_m)(2/3)(4/128)$, q=.1248 and r=.0002, and the same number of grid points were used as the former simulation.

The results shown in Fig. 12 clearly indicate a temporary existence of a regular alternate disposition of weak and strong vortices at an early stage of the time.

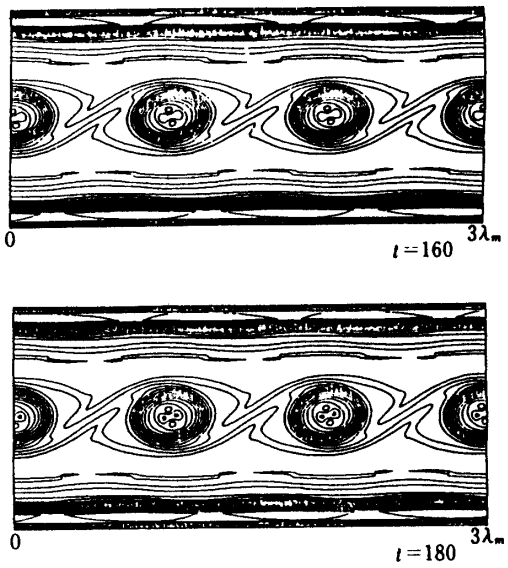

Fig. 8. Temporal evolution of the vorticity contours obtained by the present method with step 0.04 from t=160 to 180.
(monochronic initial disturbance and cyclic boundary condition are adopted)

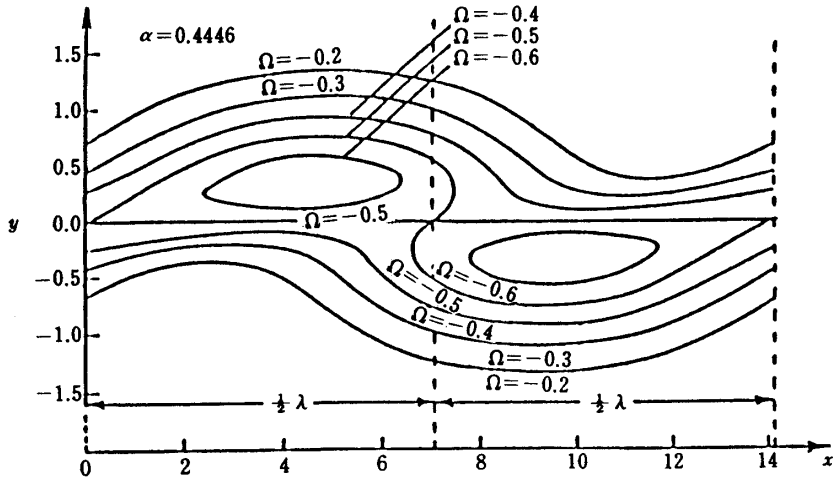

Fig. 9. Vorticity contours obtained by small disturbance theory (from Ref. [15]).

However, as the time elapses, the weak vortices are gradually stretched by the strong ones on both sides, and, finally, they are entirely rolled up into the strong vortices. Therefore, it seems that there can be observed only two strong roll-ups of vortex sheet that resemble the asymptotic state of the simulation made with the monochronic disturbance. From now on, this type of merging process is called as "the weak-strong merging."

4–4 Simulations with random disturbances

In this section, the simulation is made using either a cyclic or a flow-out boundary

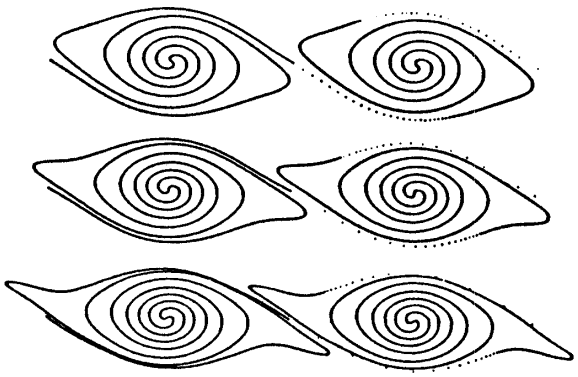

Fig. 10. asymptotic behavior of the rolled up vortex sheet by vortex method (from Ref. [16]).

condition with a random disturbance in order to examine the change in the flow field involving the merging vortices due to the disturbances.

In case of simulation under the cyclic boundary condition, the calculation conditions were the same as those for the former simulation, and the initial condition for vorticity was given by

$$\zeta=\zeta_0+A(R-.5)\exp(-\alpha_m y^2), \tag{4-4-1}$$

where R is uniform random number in (0, 1) and ζ_0 is the same as given in Eqs. (4–2). The initial condition for ψ was given by

$$\psi=\psi_0+\psi', \tag{4-4-2}$$

where ψ' was obtained by solving the equation

$$\nabla^2\psi'=A(R-.5)\exp(-\alpha_m y^2),$$

ψ_0 is the same as in Eqs. (4–2), and the amplitude A was set equal to 10^{-2}.

In the case of the cyclic boundary condition with a random disturbance, the flow field undergoes very complicated modifications in the transient process of merging vortices, as is seen in Fig. 13. In the early stage, detailed examination of the numerical results reveals a fact that only the disturbances having wavenumbers near α_m are so intensified as to play the main role in determining the intermediate regime of the shear layer, whereas the disturbances having higher or lower wavenumbers are not so developed enough as to have significant effect on the flow field. The flow pattern observed in existing experiments seems presumably to be shaped in this way. As the time elapses, even the disturbances with rather small growth rate have grown up to be strong enough to affect the intermediate regime of the vortex merging. Finally, the intensified vortex thus formed through the merging process staggers back and forth in the shear layer and fills the flow field with torn vortex sheet.

The simulation starting with a random disturbance under the flow-out boundary

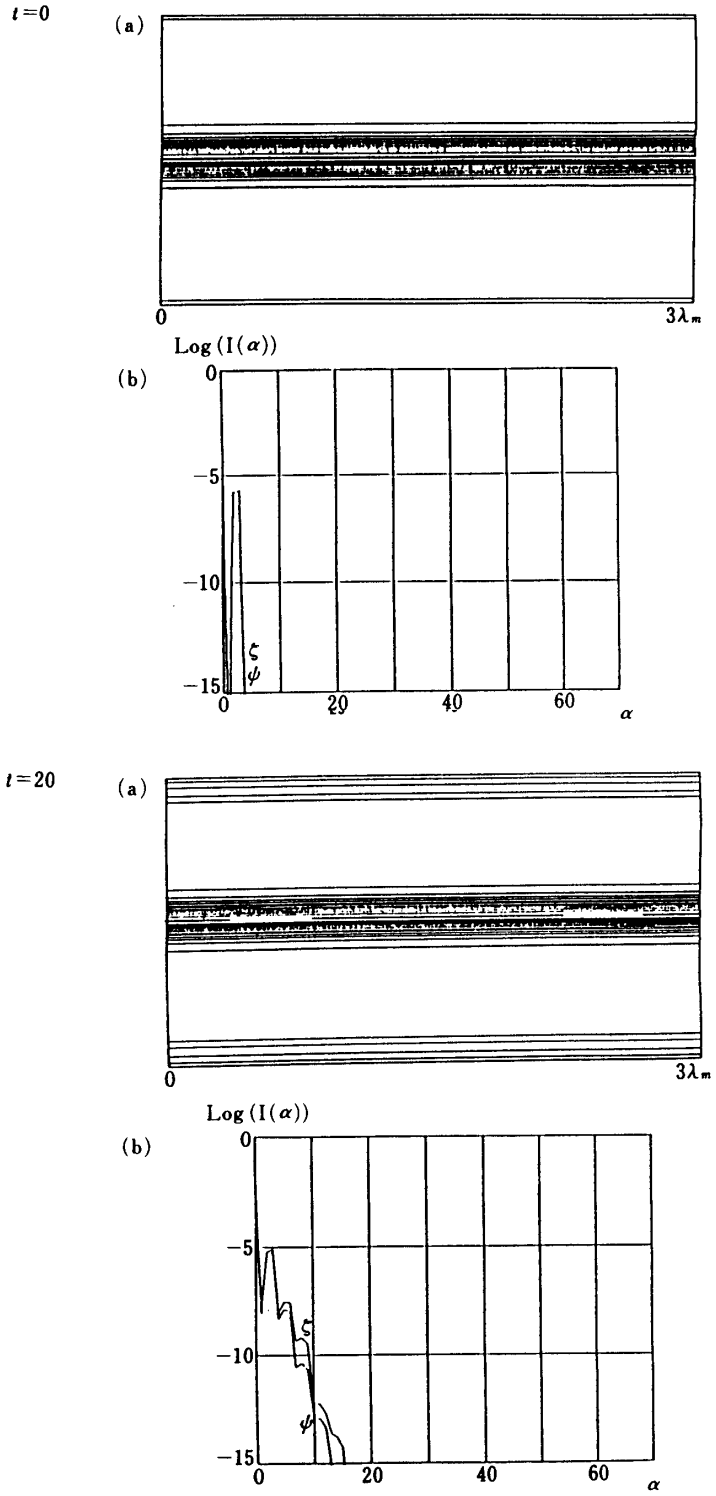

Fig. 11. (a) vorticity contours of merging vorticies obtained by the present method with interval 0.04.
(b) its Fourier analysis in x-direction. t=0 to 20 (continued).
(cyclic boundary condition is adopted)

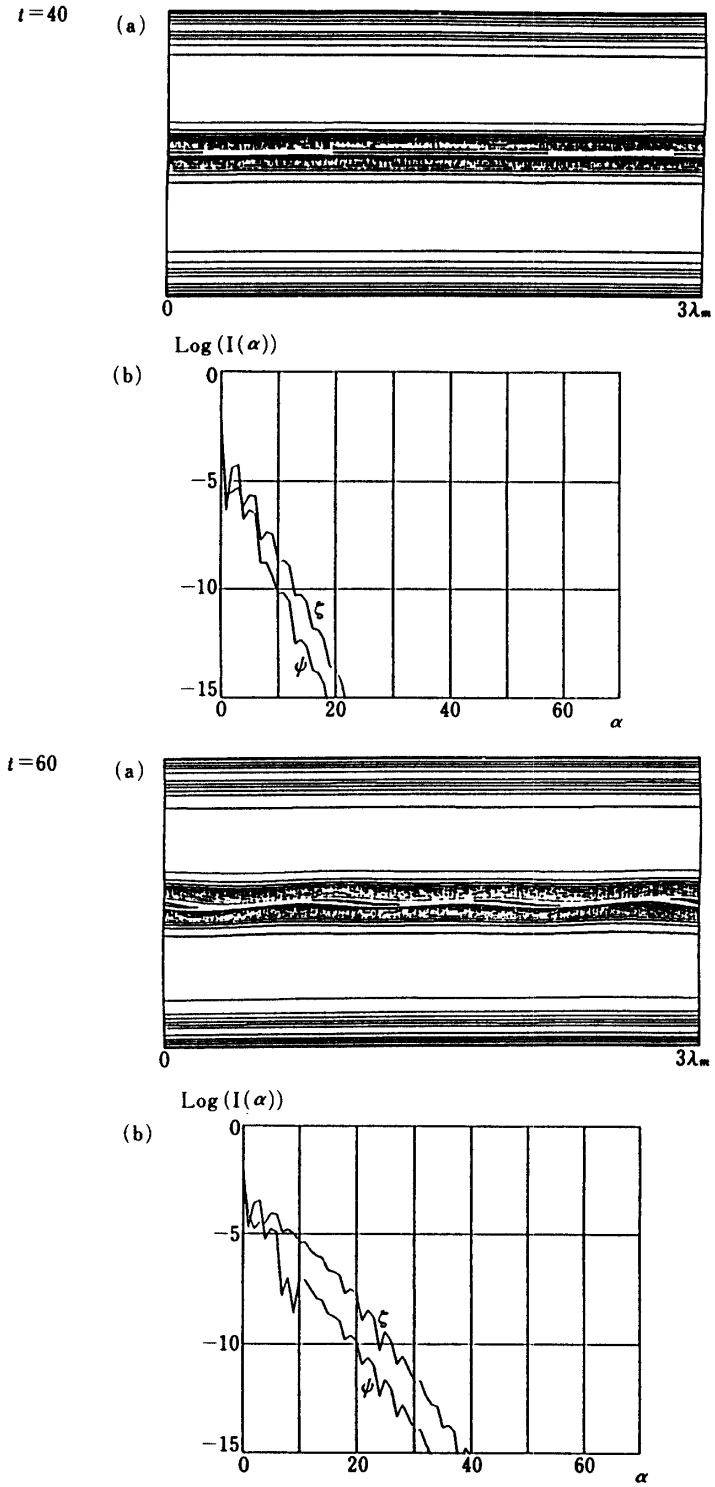

Fig. 11. (a) Vorticity contours of merging vorticies obtained by the present method with interval 0.04.
(b) its Fourier analysis in x-direction. t=40 to 60 (continued).
(cyclic boundary condition is adopted)

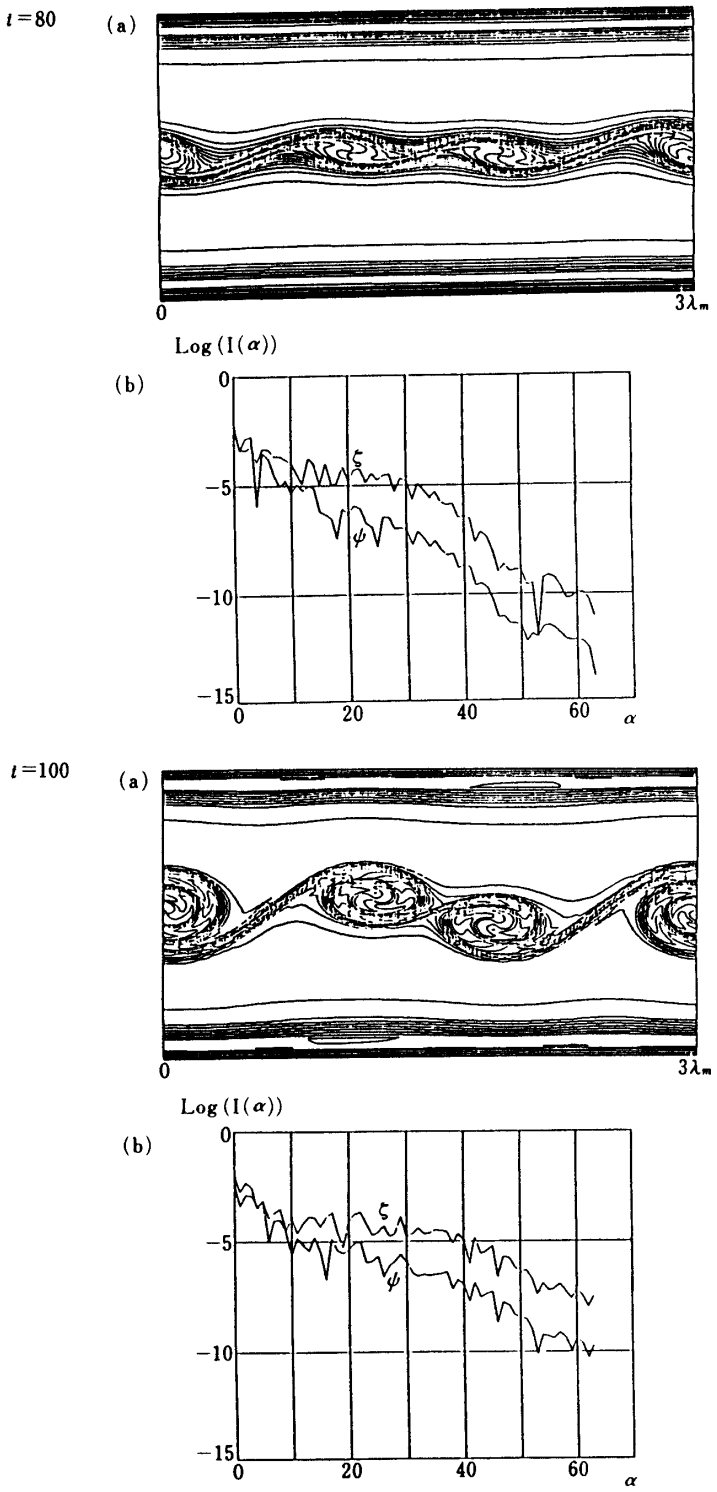

Fig. 11. (a) Vorticity contours of merging vorticies obtained by the present method with interval 0.04.
(b) its Fourier analysis in x-direction. t=80 to 100 (continued).
(cyclic boundary condition is adopted)

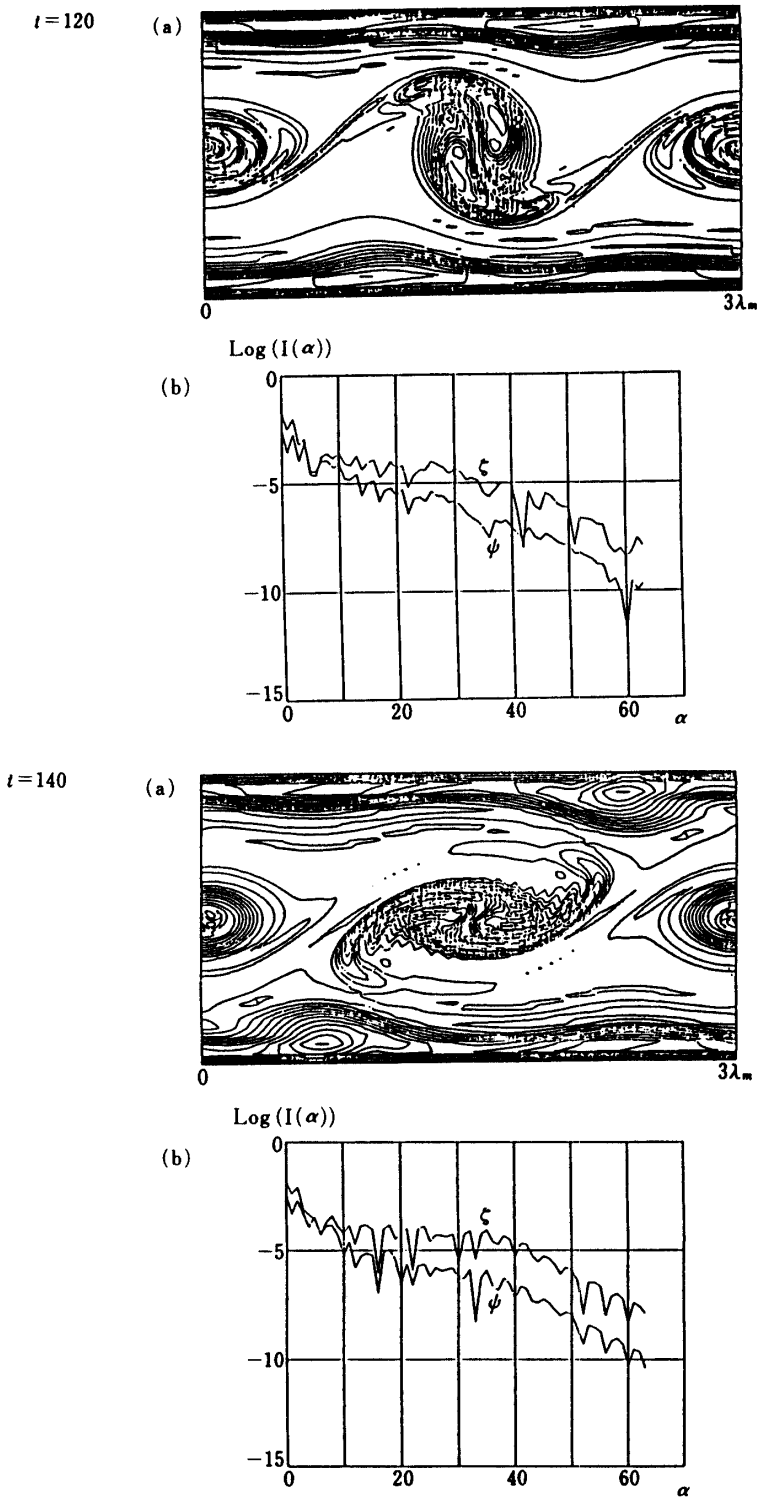

Fig. 11. (a) Vorticity contours of merging vorticies obtained by the present method with interval 0.04.
(b) its Fourier analysis in x-direction. t=120 to 140 (continued).
(cyclic boundary condition is adopted)

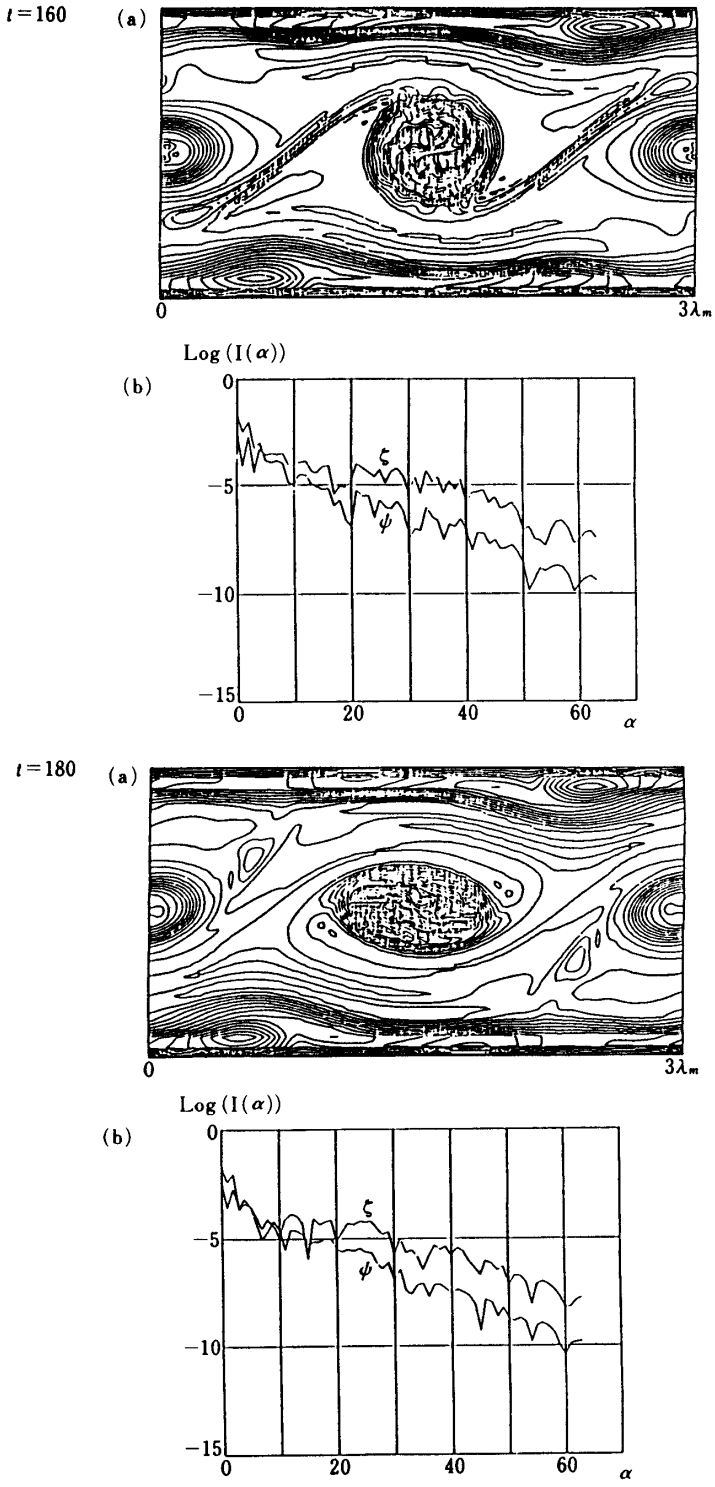

Fig. 11. (a) Vorticity contours of merging vorticies obtained by the present method with interval 0.04.
(b) its Fourier analysis in x-direction. t=160 to 180 (continued).
(cyclic boundary condition is adopted)

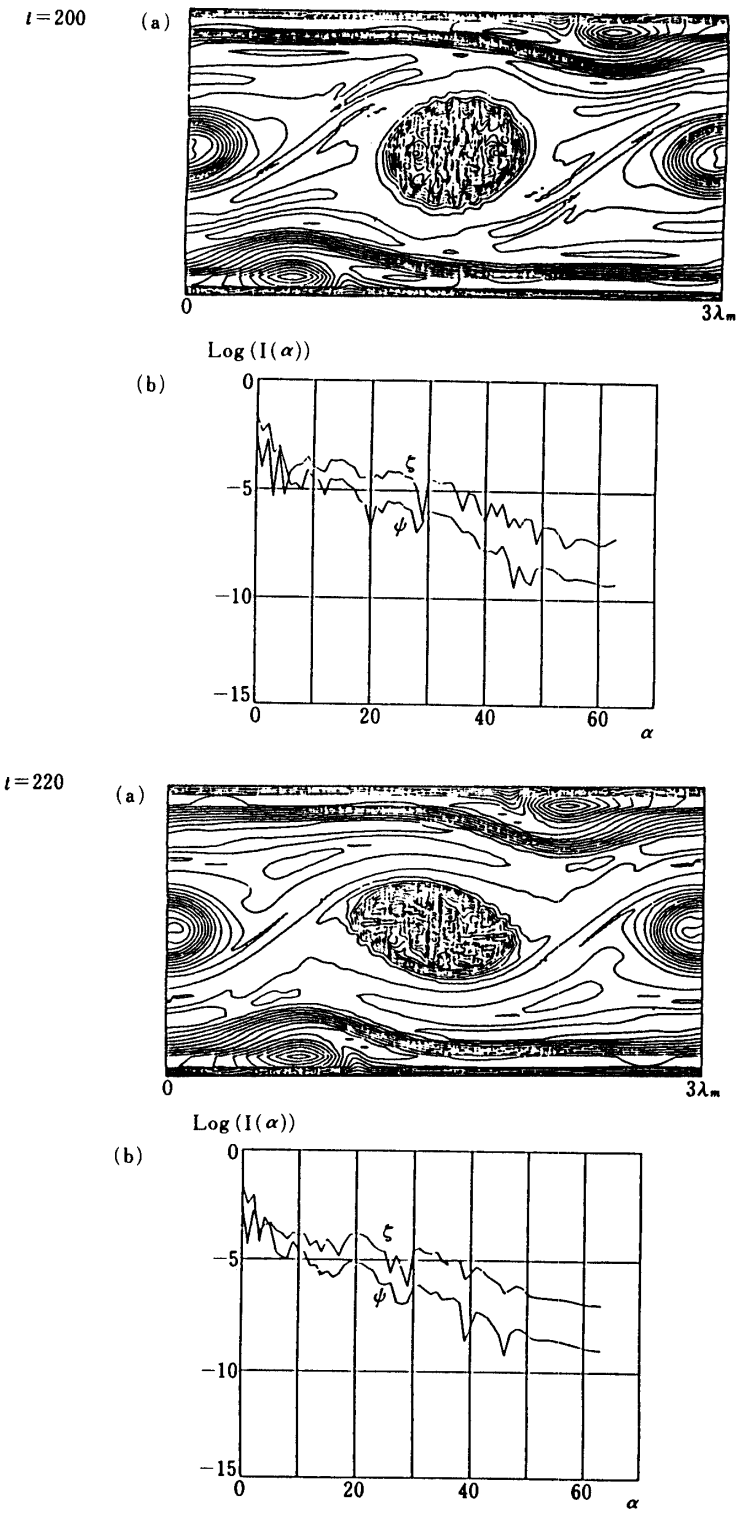

Fig. 11. (a) Vorticity contours of merging vorticies obtained by the present method with interval 0.04.
(b) its Fourier analysis in x-direction. t=200 to 220.
(cyclic boundary condition is adopted)

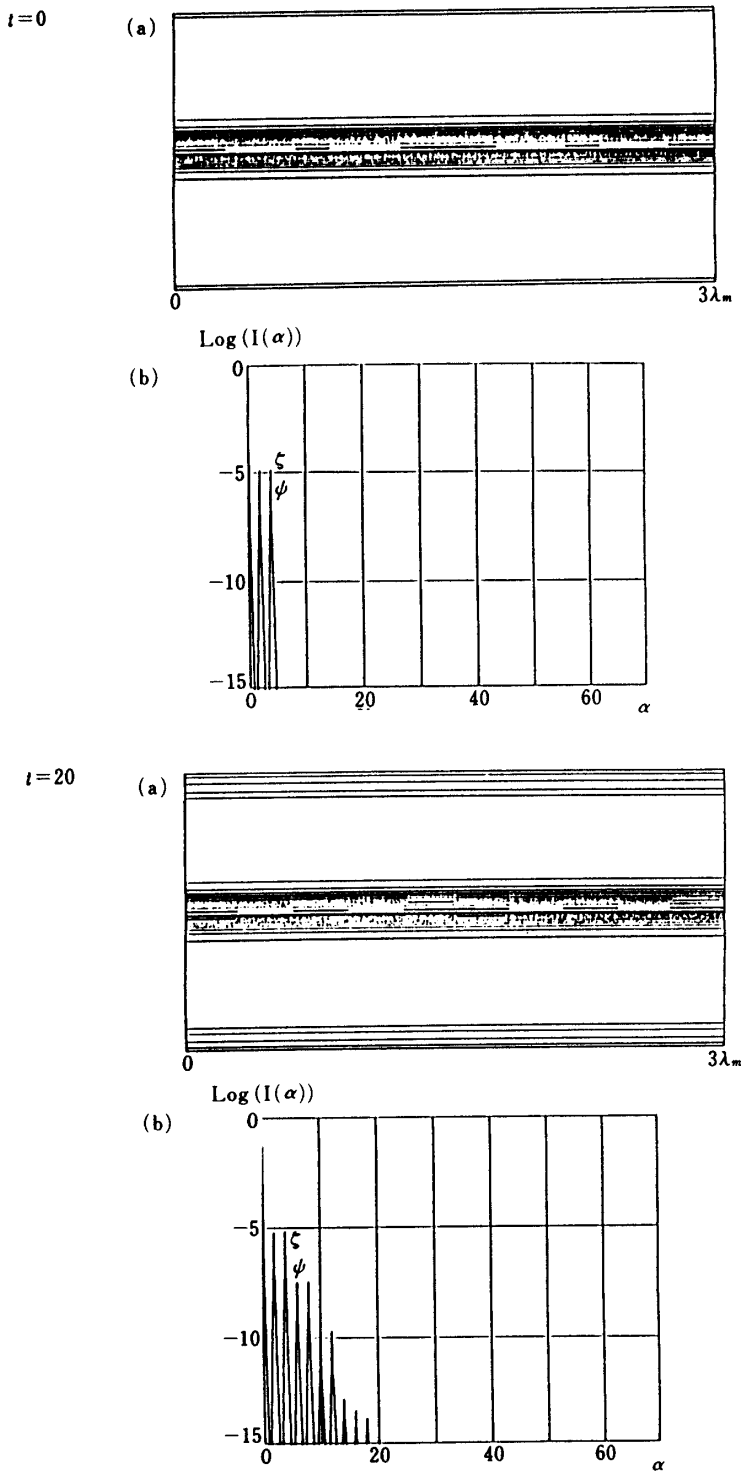

Fig. 12. (a) Vorticity contours of stretching vorticies obtained by the present method with interval 0.04. (b) its fourier analysis in x-direction. t=0 to 20 (continued).
(cyclic boundary condition is adopted)

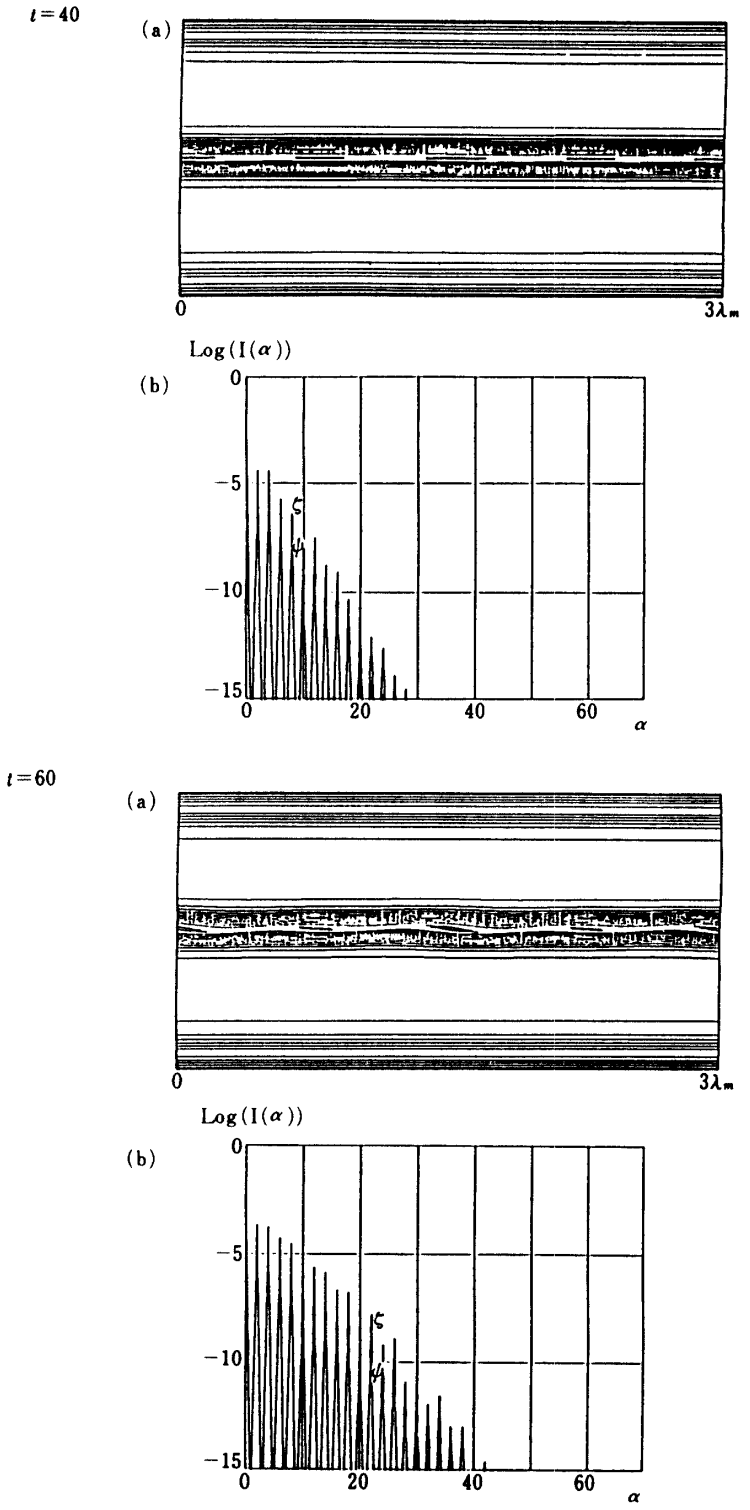

Fig. 12. (a) Vorticity contours of stretching vorticies obtained by the present method with interval 0.04. (b) its fourier analysis in x-direction. t=40 to 60 (continued).
(cyclic boundary condition is adopted)

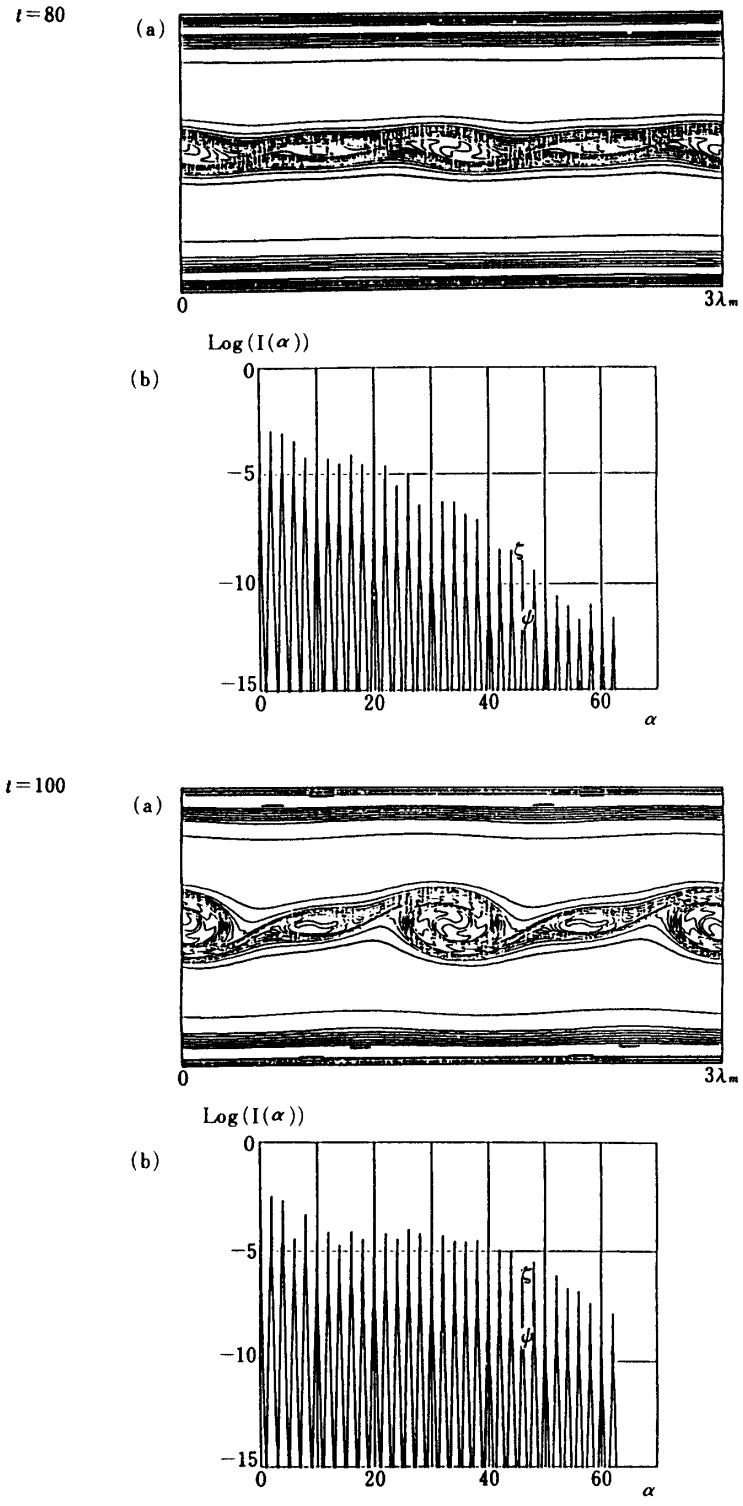

Fig. 12. (a) Vorticity contours of stretching vorticies obtained by the present method with interval 0.04. (b) its fourier analysis in x-direction. t=80 to 100 (continued).
(cyclic boundary condition is adopted)

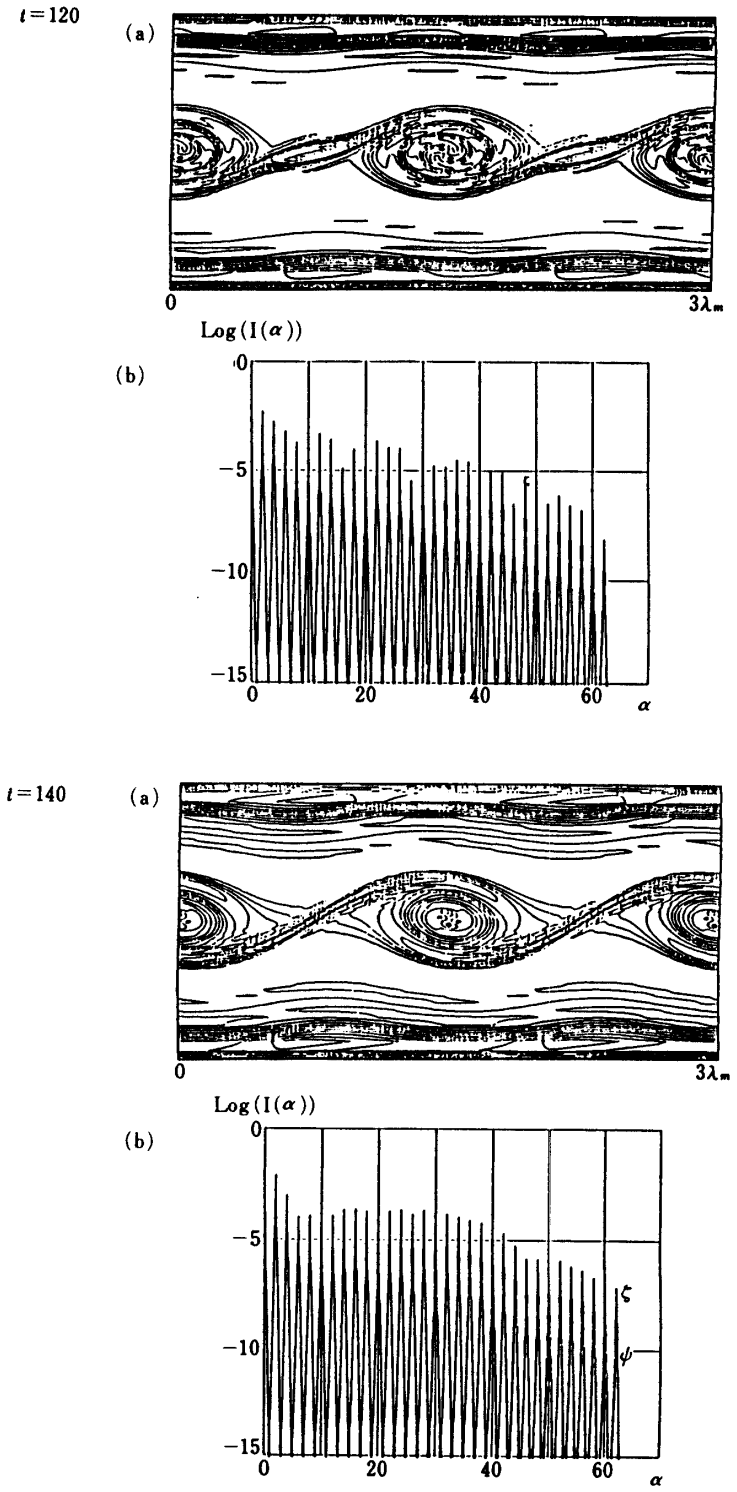

Fig. 12. (a) Vorticity contours of stretching vorticies obtained by the present method with interval 0.04. (b) its fourier analysis in x-direction. t=120 to 140 (continued).
(cyclic boundary condition is adopted)

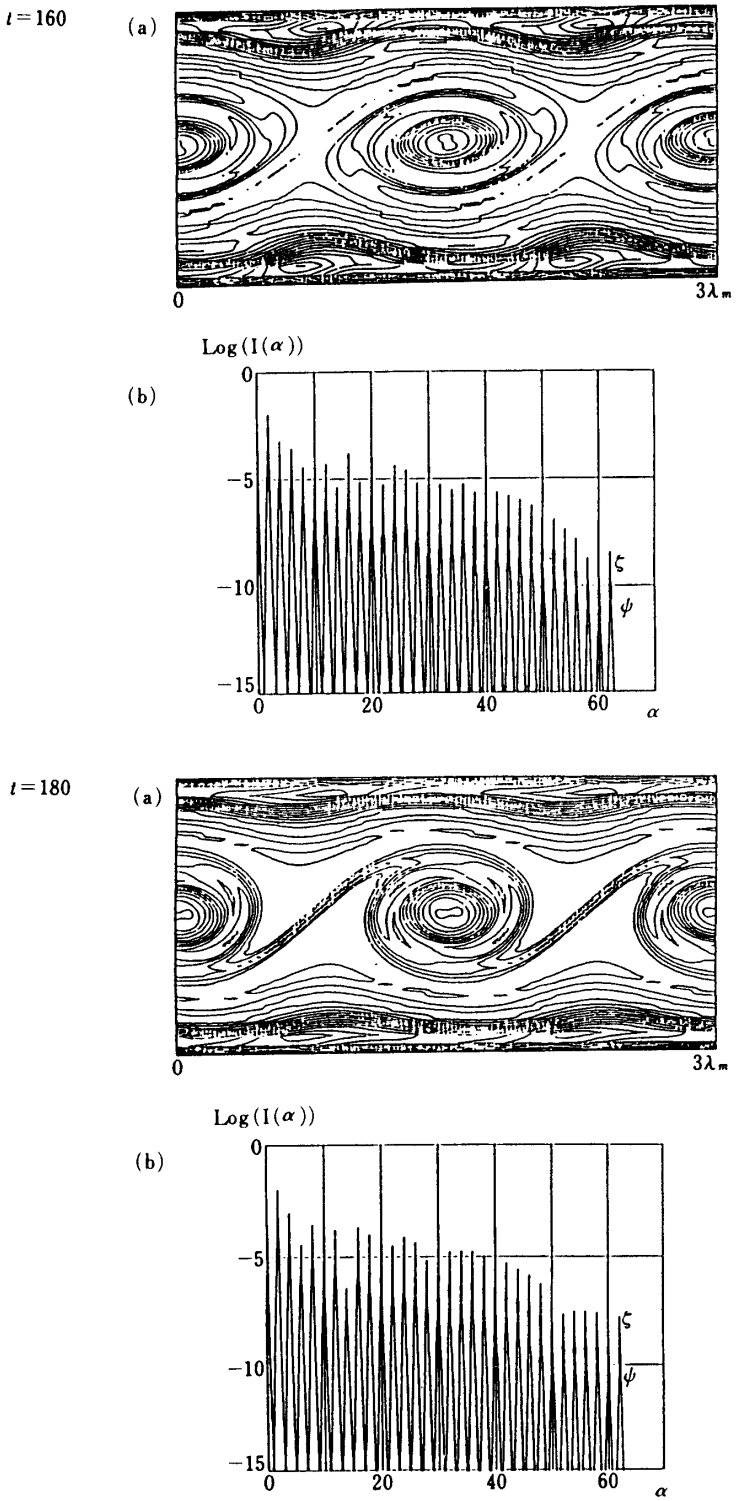

Fig. 12. (a) Vorticity contours of stretching vorticies obtained by the present method with interval 0.04. (b) its fourier analysis in x-direction. t=160 to 180 (continued).
(cyclic boundary condition is adopted)

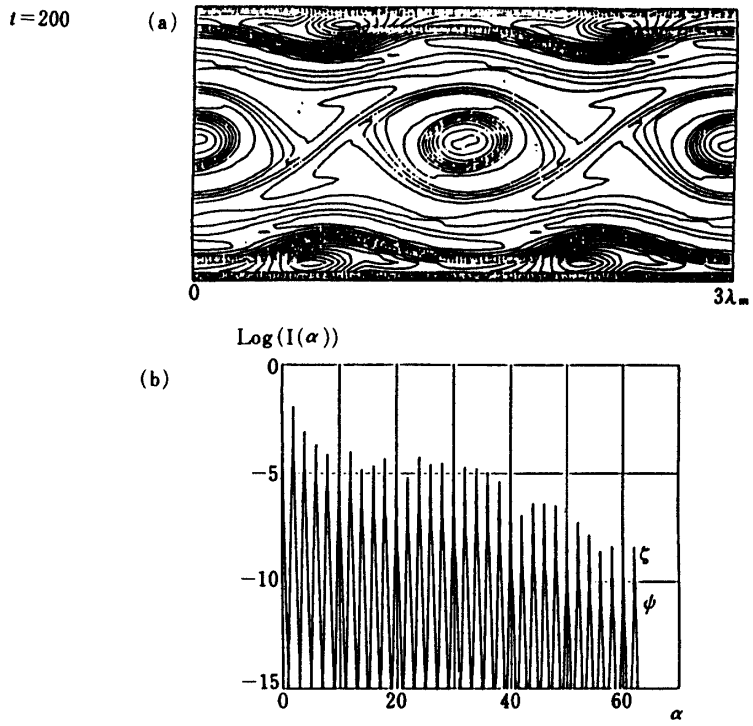

Fig. 12. (a) Vorticity contours of stretching vorticies obtained by the present method with interval 0.04. (b) its fourier analysis in x-direction. t=200. (cyclic boundary condition is adopted)

condition (see Fig. 5(b)) was made to demonstrate the total image of the shear layer. The random disturbance was imposed on the initial conditions and boundary conditions along the entrance region throughout the simulation. The grid system utilized in this simulation is $256\times101(0\leqq\xi\leqq255,\ -50\leqq\eta\leqq50)$ and the coefficients in Eqs. (4–1) were set to $p=(2\pi/\alpha_m)(20/256)$, $q=.2497$ and $r=.0003$. The time increment Δ_t was .015 and the Courant number was preserved less than .2 throughout the simulation. The initial condition for shear layer was given by

$$\psi=\psi_0+\psi', \tag{4–2–3}$$

$$\zeta=\zeta_0+A(R-.5)\exp(-\alpha_m y^2), \tag{4–2–4}$$

where R is a uniform random number in (0, 1), and ζ_0 is the same as Eqs. (4–2),

$$\psi_0=-(y+\log(\cosh(y))/2),$$

where ψ' is given in the same way as the former simulation. The amplitude A was set to 10^{-2}. The entrance condition was determined in the same way as for the shear layer at every time step.

Fig. 14 shows that the only disturbances having the wave number near α_m appear, and the weak-strong merging takes place in the very early stage of the transition,

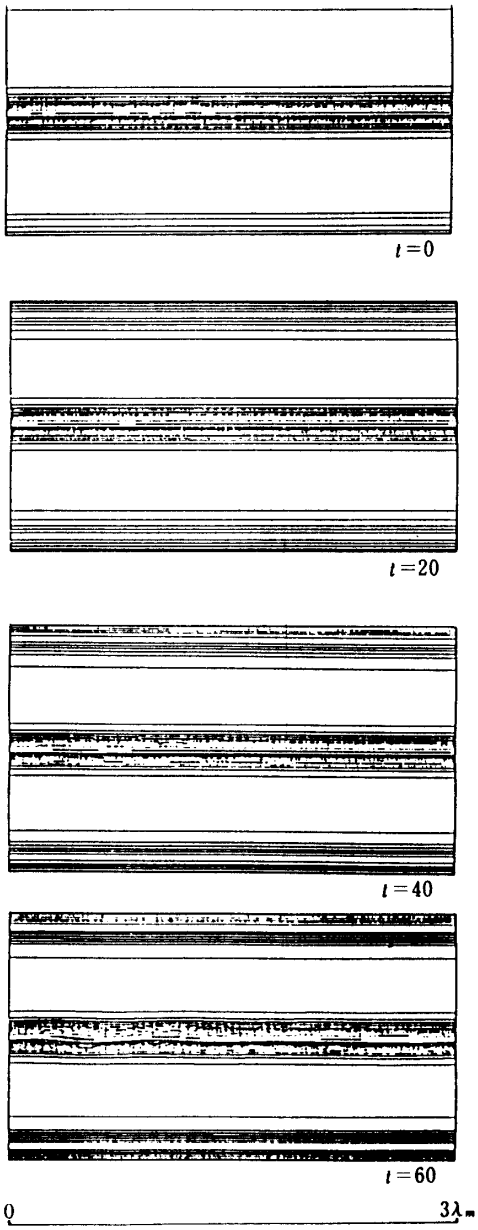

Fig. 13. Vorticity contours obtained by the present method with interval 0.04 from t=0 to 60 (continued). (random initial disturbance and cyclic boundary condition are adopted)

whereas it did not appear in the simulations obtained with cyclic boundary condition. The same intensity merging occurs intermittently in the downstream to make a intensified vortex and affects whole shear layer. Around this vortex, the torn vortex sheet is spread and the shear layer with filamented shapes are observed. This pattern is same qualitatively as can be seen in the picture proposed by Frymuth [17] (see Fig. 15).

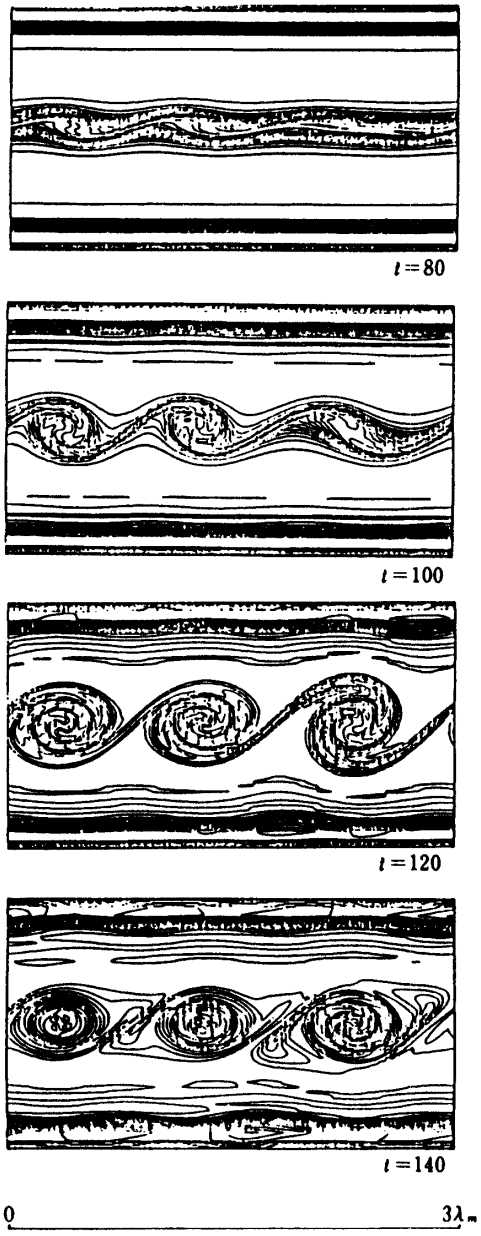

Fig. 13. Vorticity contours obtained by the present method with interval 0.04 from t=80 to 140 (continued). (random initial disturbance and cyclic boundary condition are adopted)

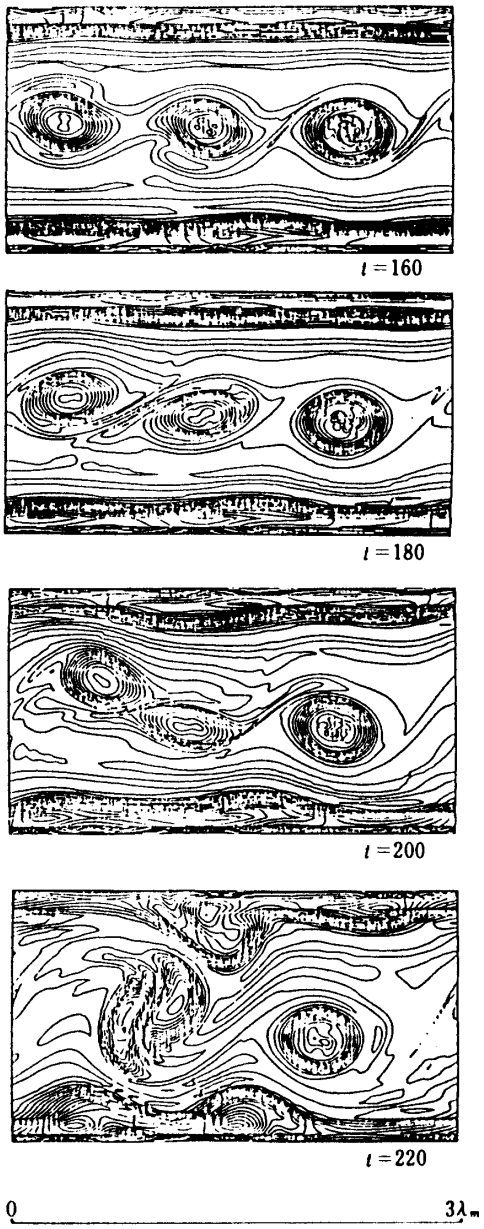

Fig. 13. Vorticity contours obtained by the present method with interval 0.04 from t=160 to 220 (continued). (random initial disturbance and cyclic boundary condition are adopted)

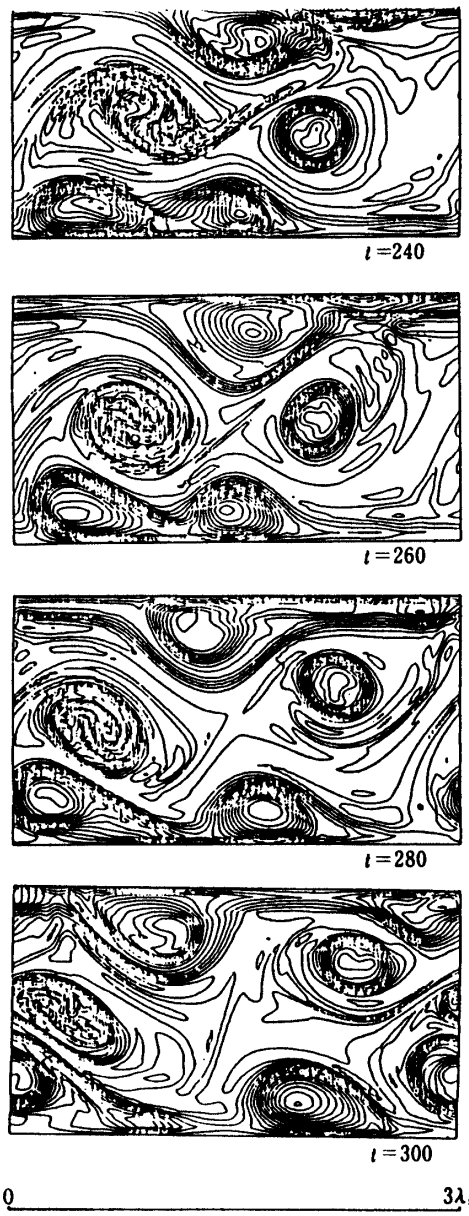

Fig. 13. Vorticity contours obtained by the present method with interval 0.04 from t=240 to 300 (continued).
(random initial disturbance and cyclic boundary condition are adopted)

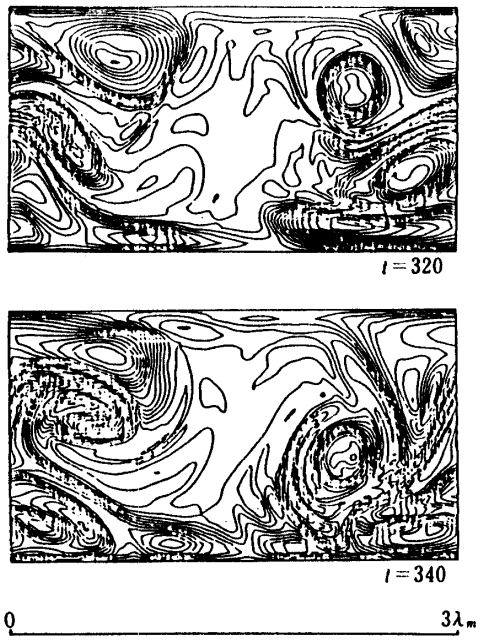

Fig. 13. Vorticity contours obtained by the present method with interval 0.04 from t=320 to 340 (continued).
(random initial disturbance and cyclic boundary condition are adopted)

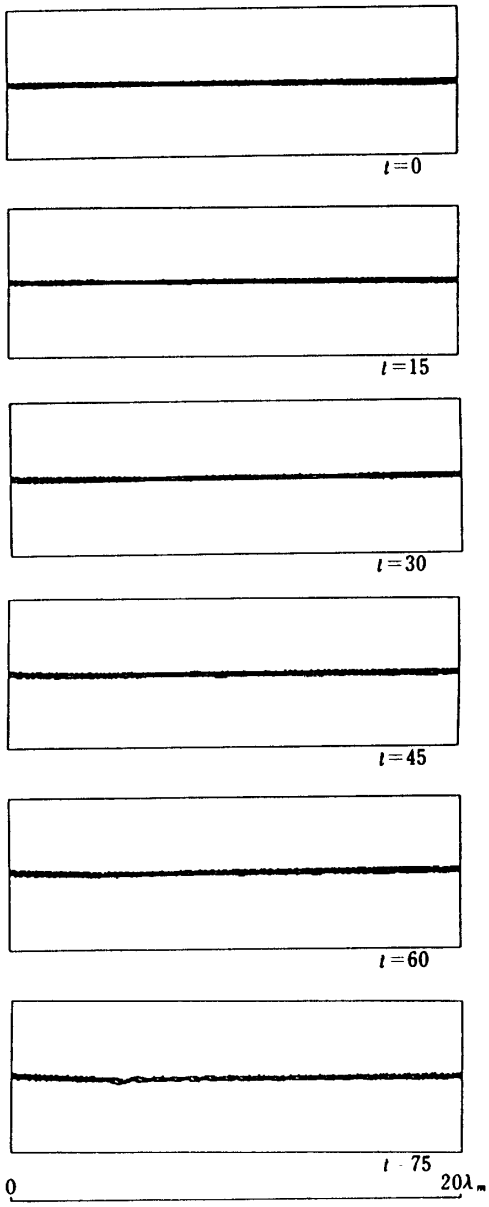

Fig. 14. Vorticity contours obtained by the present method with interval 0.04 from t=0 to 75 (continued). (flow out boundary condition and random inflow disturbance are adopted)

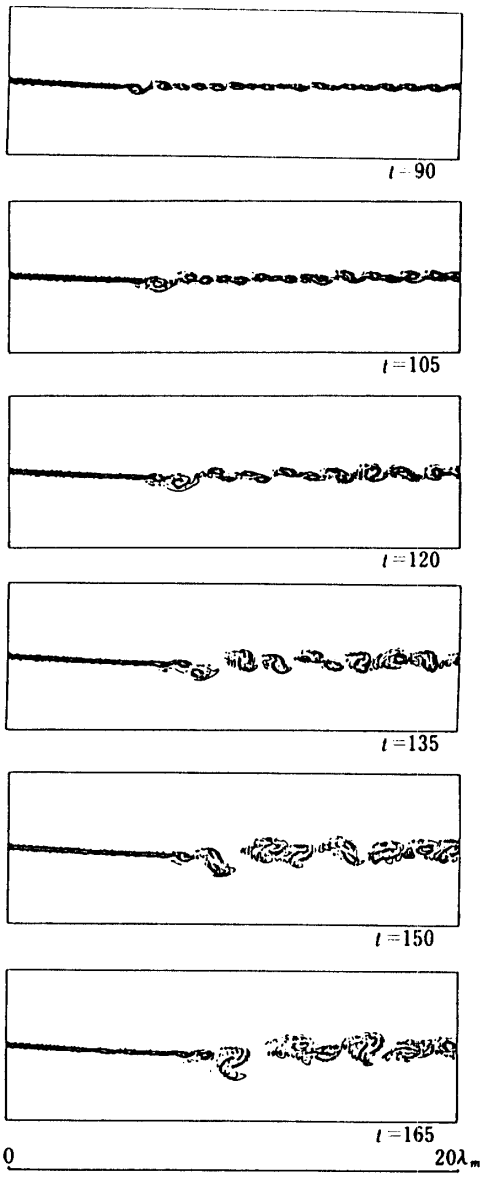

Fig. 14. Vorticity contours obtained by the present method with interval 0.04 from t=90 to 165 (continued).
(flow out boundary condition and random inflow disturbance are adopted)

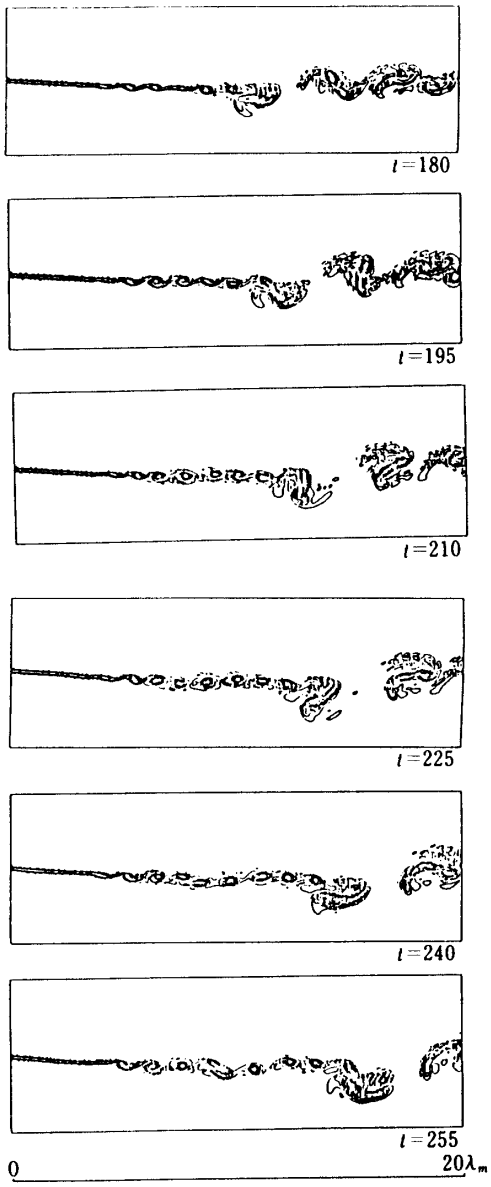

Fig. 14. Vorticity contours obtained by the present method with interval 0.04 from t=180 to 255 (continued).
(flow out boundary condition and random inflow disturbance are adopted)

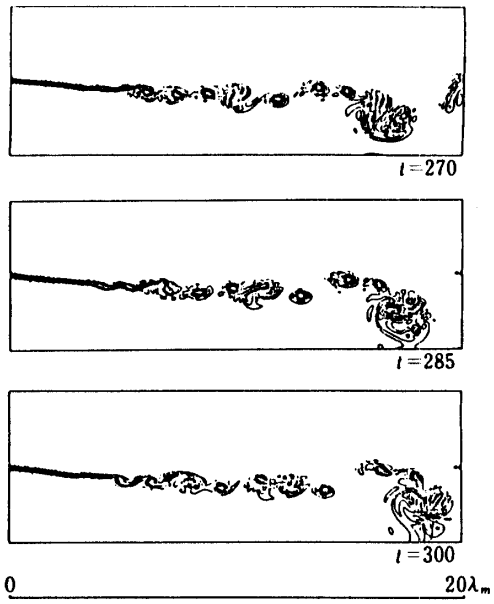

Fig. 14. Vorticity contours obtained by the present method with interval 0.04 from t=270 to 300 . (flow out boundary condition and random inflow disturbance are adopted)

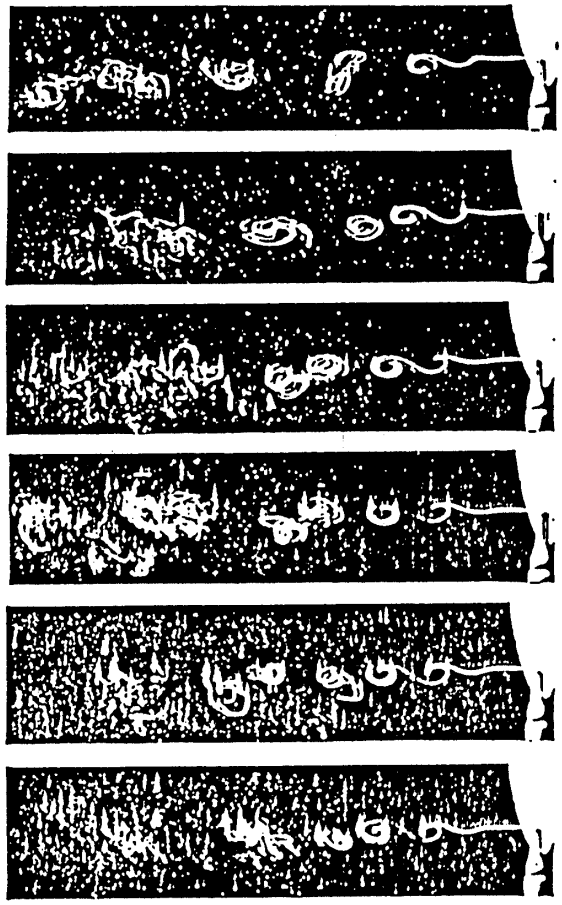

Fig. 15. A sequence of stroboscopic pictures (from Ref. [17]).

5. Concluding remarks

With emphasis on applicability to the long term integration, an improvement of higher order accuracy algorithm has been made for numerical simulation of transient shear layer for linear to nonlinear regimes. In the linear regime, the present results associated with the growth rate and vorticity contour agree well with the existing theoretical ones. Moreover, it has been shown that, in the nonlinear regime, the asymptotic behavior of vortex sheet obtained by the present simulation also indicates satisfactory agreement with the results obtained by the vortex method with the same boundary condition.

Taking the transient behavior of the shear layer from the linear to the nonlinear regimes into account, the numerical computation is carried out further to clarify the characteristic behavior of the merging vortices in the shear layer.

Finally, it is emphasized that the present algorithm proposed in view of both numerical accuracy and error isotropy is clearly superior to the existing schemes in order to predict such highly nonlinear phenomena as can be observed in the shear layer transition, etc.

6. Acknowledgement

The author would like to express his sincere gratitude to Professor K. Karashima of University Tokyo and the Institute of Space and Astronautical Science for his enlightening suggestions and encouragement. The author also appreciates Professor H. Oguchi of the Institute of Space and Astronautical Science for valuable suggestions to the unsteady phenomena in the shear layer.

Appendix A. The mechanism of aliasing (from Ref. [5])

Consider an evaluation of sum of the one-dimensional convolution expressed by the equation

$$w(k)=\sum_{\substack{p+q=k \\ |p|,|q|<K}} u(p)v(q), \tag{A-1}$$

where k, p, q are integers and u(p), v(q) are in general complex. Let's define the discrete Fourier transform of a set of N complex numbers z(k) in the region $|k|\leqq(1/2)N$, where N is assumed to have no special relation to the cutoff K in Eq. (A-1). Since z(k) indicates a field in "wave-vector" space, its Fourier transform exists in "physical" space. The grid points are defined by the equation

$$x_j=2\pi j/N, \tag{A-2}$$

where $j=0, 1,.., N-1$. If the discrete Fourier transform Z_j of z(k) is defined as

$$Z_j=\sum_{|k|\leqq\frac{1}{2}N} z(k)\exp(ikx_j),\ (j=0,\ 1,..,N-1). \tag{A-3}$$

Then, it follows from the nature of roots of unity that

$$\sum_{j=0}^{N-1}\exp(i(k-p)x_j)=\begin{cases}N & \text{if } k\equiv p(\text{mod } N)\\ 0 & \text{otherwise}\end{cases} \tag{A-4}$$

Therefore, the inverse transform to Eq. (A-3) is given as

$$z(k)=\frac{1}{N}\sum_{j=0}^{N-1} Z_j \exp\ (-ikx_j)\ (|k|\leqq\frac{1}{2}N). \tag{A-5}$$

It is evident that Eq. (A-3) is algebraically equivalent to Eq. (A-5).

The most obvious way to try to get a discrete convolution theorem for calculation of Eq. (A-1) is to introduce the physical-space transform $\hat{U}_j$, $\hat{V}_j$ of the spectral fields u(k), v(k), respectively, by means of the discrete Fourier transform, Eq. (A-3), together with the condition N=2K. Here $\hat{U}_j$, $\hat{V}_j$ are defined at the 2K points of $x_j=2\pi j/(2K)$ for j=0, 1,.., 2K−1, and the domains of the definition for u(k) and v(k) are extended to $|k|\leqq K$, where u(−K)=v(−K)=0 has been required to validate Eq. (A-3). If $\hat{W}_j$ is defined as the local product $\hat{U}_j\hat{V}_j$ of the transformed fields for j=0, 1,.., 2K−1 and Eq. (A-5) is used with N=2K to compute the inverse transform $\hat{w}_j$ of $\hat{W}_j$ for $|k|\leqq K$, then, it gives

$$\begin{aligned}\hat{w}(k)&=\frac{1}{2K}\sum_{j=0}^{2K-1}\Big\{\sum_{p\leqq K} u(p)\exp(ipx_j)\sum_{q\leqq K} v(q)\exp(iqx_j)\Big\}\exp(-ikx_j)\\ &=\sum_{p,q\leqq K} u(p)v(q)\frac{1}{N}\sum_{j=0}^{K-1}\exp(i(p+q-k)x_j),\end{aligned} \tag{A-6}$$

which can be further reduced by application of Eq. (A-4) to

$$\hat{w}(k)=w(k)+w(k+2K)+w(k-2K)\ (|k|\leqq K), \tag{A-6′}$$

where w(k) has been given by Eq. (A-1). The last two terms of Eq. (A-6′) result from the cyclic relation expressed by $\exp(i(k+N)x_j)=\exp(ikx_j)$ for all integers j and k, and the discrete grid points x_j do not distinguish the wave-vector k from its "aliases" k±N and k±2N, etc. It must be noted that one of the two terms in Eq. (A-6), which result from the aliasing, cannot at least be zero for any $|k|\leqq K$.

In the conventional finite difference shcemes, aliasing will presumably occur in the wave numbers less than N/2, because they cannot be distinguished from the wave numbers in the higher range than N/2. Because of this, the cut off wave number should be set less than N/2 in order to evade aliasing.

Appendix B. Components of finite difference approximation for the Jacobian

Components of the finite difference approximation for the Jacobian used in the present method are given as follows:

$$J^{++}_{CW}=\frac{1}{20\Delta^2}\{(\zeta_{i+2,j-1}-\zeta_{i-2,j+1})(\psi_{i+1,j+2}-\psi_{i-1,j-2})$$
$$-(\zeta_{i+1,j+2}-\zeta_{i-1,j-2})(\psi_{i+2,j-1}-\psi_{i-2,j+1})\},$$

$$J^{+*}_{CW}=\frac{1}{20\Delta^2}\{\zeta_{i+2,j-1}(\psi_{i+3,j+1}-\psi_{i+1,j-3})-\zeta_{i-2,j+1}(\psi_{i-1,j+3}-\psi_{i-3,j-1})$$
$$-\zeta_{i+1,j+2}(\psi_{i+3,j+1}-\psi_{i-1,j+3})+\zeta_{i-1,j-2}(\psi_{i+1,j-3}-\psi_{i-3,j-1})\},$$

$$J^{*+}_{CW}=\frac{1}{20\Delta^2}\{\zeta_{i+3,j+1}(\psi_{i+1,j+2}-\psi_{i+2,j-1})-\zeta_{i-3,j-1}(\psi_{i-2,j+1}-\psi_{i-1,j-2})$$
$$-\zeta_{i-1,j+3}(\psi_{i+1,j+2}-\psi_{i-2,j+1})+\zeta_{i+1,j-3}(\psi_{i+2,j-1}-\psi_{i-1,j-2})\},$$

$$J^{++}_{CW\pi/4}=\frac{1}{40\Delta^2}\{(\zeta_{i+3,j+1}-\zeta_{i-3,j-1})(\psi_{i-1,j+3}-\psi_{i+1,j-3})$$
$$-(\zeta_{i-1,j+3}-\zeta_{i+1,j-3})(\psi_{i+3,j+1}-\psi_{i-3,j-1})\},$$

$$J^{+*}_{CW\pi/4}=\frac{1}{40\Delta^2}\{\zeta_{i+3,j+1}(\psi_{i+2,j+4}-\psi_{i+4,j-2})-\zeta_{i-3,j-1}(\psi_{i-4,j+2}-\psi_{i-2,j-4})$$
$$-\zeta_{i-1,j+3}(\psi_{i+2,j+4}-\psi_{i-4,j+2})+\zeta_{i+1,j-3}(\psi_{i+4,j-2}-\psi_{i-2,j-4})\},$$

$$J^{*+}_{CW\pi/4}=\frac{1}{40\Delta^2}\{\zeta_{i+4,j-2}(\psi_{i+3,j+1}-\psi_{i+1,j-3})-\zeta_{i-4,j+2}(\psi_{i-1,j+3}-\psi_{i-3,j-1})$$
$$-\zeta_{i+2,j+4}(\psi_{i+3,j+1}-\psi_{i-1,j+3})+\zeta_{i-2,j-4}(\psi_{i+1,j-3}-\psi_{i-3,j-1})\},$$

$$J^{++}_{AW}=\frac{1}{20\Delta^2}\{(\zeta_{i+2,j+1}-\zeta_{i-2,j-1})(\psi_{i-1,j+2}-\psi_{i+1,j-2})$$
$$-(\zeta_{i-1,j+2}-\zeta_{i+1,j-2})(\psi_{i+2,j+1}-\psi_{i-2,j-1})\},$$

$$J^{+*}_{AW}=\frac{1}{20\Delta^2}\{\zeta_{i+2,j+1}(\psi_{i+1,j+3}-\psi_{i+3,j-1})-\zeta_{i-2,j-1}(\psi_{i-3,j+1}-\psi_{i-1,j-3})$$
$$-\zeta_{i-1,j+2}(\psi_{i+1,j+3}-\psi_{i-3,j+1})+\zeta_{i+1,j-2}(\psi_{i+3,j-1}-\psi_{i-1,j-3})\},$$

$$J^{*+}_{AW}=\frac{1}{20\Delta^2}\{\zeta_{i+1,j+3}(\psi_{i-1,j+2}-\psi_{i+2,j+1})-\zeta_{i-1,j-3}(\psi_{i-2,j-1}-\psi_{i+1,j-2})$$
$$-\zeta_{i-3,j+1}(\psi_{i-1,j+2}-\psi_{i-2,j-1})+\zeta_{i+3,j-1}(\psi_{i+2,j+1}-\psi_{i+1,j-2})\},$$

$$J^{++}_{AW\pi/4}=\frac{1}{40\Delta^2}\{(\zeta_{i+1,j+3}-\zeta_{i-1,j-3})(\psi_{i-3,j+1}-\psi_{i+3,j-1})$$
$$-(\zeta_{i-3,j+1}-\zeta_{i+3,j-1})(\psi_{i+1,j+3}-\psi_{i-1,j-3})\},$$

$$J^{+*}_{AW\pi/4}=\frac{1}{40\Delta^2}\{\zeta_{i+1,j+3}(\psi_{i-2,j+4}-\psi_{i+4,j+2})-\zeta_{i-1,j-3}(\psi_{i-4,j-2}-\psi_{i+2,j-4})$$
$$-\zeta_{i-3,j+1}(\psi_{i-2,j+4}-\psi_{i-4,j-2})+\zeta_{i+3,j-1}(\psi_{i+4,j+2}-\psi_{i+2,j-4})\},$$

$$J^{*+}_{AW\pi/4}=\frac{1}{40\Delta^2}\{\zeta_{i+4,j+2}(\psi_{i+1,j+3}-\psi_{i+3,j-1})-\zeta_{i-4,j-2}(\psi_{i-3,j+1}-\psi_{i-1,j-3})$$
$$-\zeta_{i-2,j+4}(\psi_{i+1,j+3}-\psi_{i-3,j+1})+\zeta_{i+2,j-4}(\psi_{i+3,j-1}-\psi_{i-1,j-3})\},$$

where subscripts CW and AW denote the value in the new coordinates obtained through rotation of the original coordinates in either clockwise or anti-clockwise by arctan(1/2) radian, respectively, and the subscript $\pi/4$ indicates the rotation angle in radian.

Appendix C. Equivalence of energy conservation to the third Jacobian constraint.

The third Jacobian constraint is expressed as

$$\overline{\psi\zeta_t}=\overline{\psi\ J(\psi,\ \zeta)}=0, \tag{C-1}$$

where the barred quantities denote the average over the domain. The left hand side of Eq. (C-1) is transformed into Eq. (C-2) given by

$$\overline{\psi\zeta_t}=\overline{(\psi\zeta)_t}-\overline{(\psi_t\zeta)}. \tag{C-2}$$

The first term in the right hand side of Eq. (C-2) will be re-expressed as,

$$\overline{\psi\zeta}=\overline{\psi(\psi_{xx})+\psi(\psi_{yy})}=\overline{(\psi\psi_x)_x+(\psi\psi_y)_y}-\overline{(\psi_x^2+\psi_y^2)}. \tag{C-3}$$

The second term of the right hand side of Eq. (C-3) will be interpreted as two times of kinetic energy, and Gauss' divergent theorem will be applied to the first term of the right hand side of Eq. (C-3). Thus, Eq. (C-3) becomes

$$\overline{\psi\zeta}=-2\overline{E}. \tag{C-4}$$

Substitution of Eq. (C-4) into Eq. (C-2) lead to

$$\overline{\psi\zeta_t}=-2\overline{E_t}-\overline{\psi_t\zeta}. \tag{C-5}$$

Application of Green's theorem to ψ and ψ_t, together with additional assumption that there is neither inflow nor out-flow of the invariants through the boundary, gives the following relation

$$\int_v(\psi_t\nabla^2\psi-\psi\nabla^2\psi_t)dv=\int_{\partial v}\left[\psi_t\frac{\partial\psi}{\partial n}-\psi\left(\frac{\partial\psi}{\partial n}\right)_t\right]ds=0. \tag{C-6}$$

From Eq. (C-6), it follows that

$$\int_v \psi_t \nabla^2 \psi dv = \int_v \psi \nabla^2 \psi_t dv. \tag{C-7}$$

Thus, $\overline{\psi\zeta_t}=0$ is equivalent to $\overline{E_t}=0$

Appendix D. 9-points finite difference approximation

Finite difference approximation of the differential coefficients can be formulated as follows;

$$\begin{pmatrix} \Delta f^{i} \\ \Delta^2 f^{ii} \\ \Delta^3 f^{iii} \\ \Delta^4 f^{iv} \\ \Delta^5 f^{v} \\ \Delta^6 f^{vi} \\ \Delta^7 f^{vii} \\ \Delta^8 f^{viii} \end{pmatrix} = \begin{pmatrix} \frac{-1}{280}, & \frac{4}{105}, & \frac{-1}{5}, & \frac{4}{5}, & \frac{-4}{5}, & \frac{1}{5}, & \frac{-4}{105}, & \frac{1}{280} \\ \frac{-1}{560}, & \frac{8}{315}, & \frac{-1}{5}, & \frac{8}{5}, & \frac{8}{5}, & \frac{-1}{5}, & \frac{8}{315}, & \frac{-1}{560} \\ \frac{7}{240}, & \frac{-3}{10}, & \frac{169}{120}, & \frac{-61}{30}, & \frac{61}{30}, & \frac{-169}{120}, & \frac{3}{10}, & \frac{-7}{240} \\ \frac{7}{240}, & \frac{-2}{5}, & \frac{169}{60}, & \frac{-122}{15}, & \frac{-122}{15}, & \frac{169}{60}, & \frac{-2}{5}, & \frac{7}{240} \\ \frac{-1}{6}, & \frac{3}{2}, & \frac{-13}{3}, & \frac{29}{6}, & \frac{-29}{6}, & \frac{13}{3}, & \frac{-3}{2}, & \frac{1}{6} \\ \frac{-1}{4}, & 3, & -13, & 29, & 29, & -13, & 3, & \frac{-1}{4} \\ \frac{1}{2}, & -3, & 7, & -7, & 7, & -7, & 3, & \frac{-1}{2} \\ 1, & -8, & 28, & -56, & -56, & 28, & -8, & 1 \end{pmatrix} \times \begin{pmatrix} f_4-f_0 \\ f_3-f_0 \\ f_2-f_0 \\ f_1-f_0 \\ f_{-1}-f_0 \\ f_{-2}-f_0 \\ f_{-3}-f_0 \\ f_{-4}-f_0 \end{pmatrix}$$

where f_n represents the value of $f((i+n)\triangle)$ and $\triangle$ is grid spacing.

Appendix E. Some comments on Kawamura's method

There are several reasons why Kawamura's method [17] is not employed in this paper, which may be summarized as follows.

i) Conservation of vorticity

Kawamura's method utilizes u, v and p as fundamental variables, for which the

governing equations are written, respectively, as follows (viscosity term is omitted),

$$u_t+uu_x+vu_y+p_x+\frac{1}{4}|u|u_{xxxx}+\frac{1}{4}|v|u_{yyyy}=0, \tag{E-1-a}$$

$$v_t+uv_x+vv_y+p_y+\frac{1}{4}|u|v_{xxxx}+\frac{1}{4}|v|v_{yyyy}=0, \tag{E-1-b}$$

$$\nabla^2 p=-\nabla\cdot(u\cdot\nabla u). \tag{E-1-c}$$

If a finite difference approximation is applied to Eq. (E-1-a) and Eq. (E-1-b) (fourth order filtering terms are omitted), then, the above equations are reduced to

$$u_t+u\sum X_{i,j}u_{i,j}+v\sum Y_{i,j}u_{i,j}+-\sum X_{i,j}p_{i,j}=0, \tag{E-2-a}$$

$$v_t+u\sum X_{i,j}v_{i,j}+v\sum Y_{i,j}v_{i,j}+-\sum Y_{i,j}p_{i,j}=0, \tag{E-2-b}$$

where $X_{i,j}$ and $Y_{i,j}$ represent coefficients of finite difference approximations of x- and y-derivatives, respectively. In the case of 2-dimensional incompressible flow, the convection equation is prescribed in the vorticity conservative form, so that Eq. (E-1) must conserve the vorticity. To examine this circumstance, differentiation of Eq. (E-2-a) with respect to y and Eq. (E-2-b) with respect to x, and, then, combining both equations gives the following relation

$$\begin{aligned}&\zeta_t+u\sum X_{i,j}\zeta_{i,j}+v\sum Y_{i,j}\zeta_{i,j}+\sum X_{i,j}(p)_y-\sum Y_{i,j}(p)_x\\&+u_x\sum X_{i,j}v_{i,j}+v_x\sum Y_{i,j}v_{i,j}-u_y\sum X_{i,j}u_{i,j}-v_y\sum Y_{i,j}u_{i,j}=0.\end{aligned} \tag{E-3}$$

The above equation can be further reduced to

$$\zeta_t+u\zeta_x+v\zeta_y+\zeta(u_x+v_y)=0. \tag{E-4}$$

From the result shown by Eq. (E-4), it is clearly known that Eq. (E-1) conserves vorticity only in the case the flow field satisfies the divergent free condition strictly.

ii) Conservation of enstrophy and energy

As has been already mentioned in chapter 3, the conventional finite difference approximation to the Jacobian does not conserve the energy and the enstrophy. Since Eq. (E-3) takes the form that is equivalent to the conventional finite difference approximation to the Jacobian, it does not conserve enstrophy and energy. In this case, if the long-term integration of 2-dimensional flow is made by use of this method, vortices with physically unreasonable value appear and the flow field gradually loses its reality (see Fig. 16).

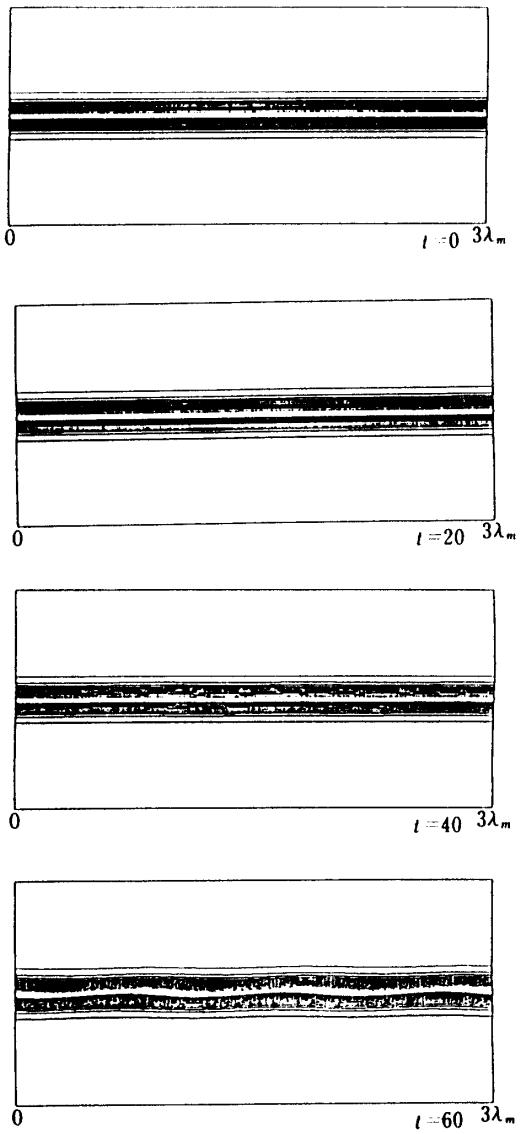

Fig. 16. Temporal evolution of the vorticity contours obtained by Kawamura's method with step 0.04 from t=0 to 60 (continued).
(monochronic initial disturbance and cyclic boundary condition are adopted)

iii) Effect of fourth order diffusion

The peculiar formulation of Kawamura's method consists in 4th-order diffusion term that is controlled by absolute value of contravaliant velocity. For this reason, if the different flow fields which are made of two different grid systems but have same convection speed, i.e. fine one and coarse one, are simulated by use of Kawamura's method, then, strong diffusion is augmented in the fine grid system, whereas weak diffusion is enhanced in the coarse grid system. Therefore, if an outer flow is computed using the conventional grid system, i.e. fine grid near the body surface and coarse grid in the far field, the strong diffusion is augmented in the fiow field near the body surface, while the very weak diffusion is enhanced in the fiow field far from the

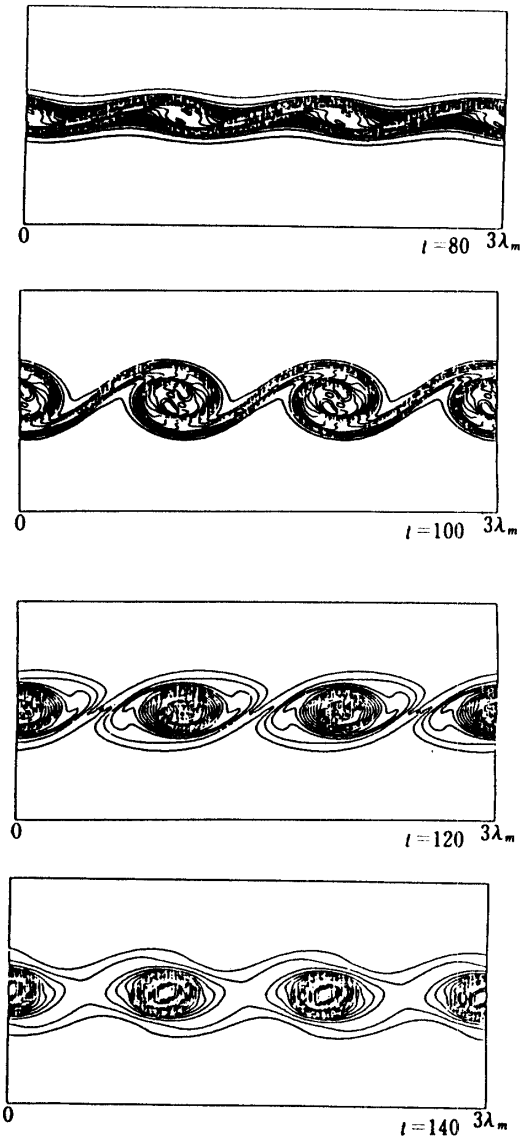

Fig. 16. Temporal evolution of the vorticity contours obtained by Kawamura's method with step 0.04 from t=80 to 140 (continued).
(monochronic initial disturbance and cyclic boundary condition are adopted)

body surface. Thus, the strong nonlinear phenomena near the body surface is stabilized by this strong diffusion and the long-term integration can be, therefore, continued without nonlinear instability. The comparison between the simulation with the fourth-order diffusion and 6th-8th order diffusion, that is same as used in present method, is shown in Fig. 17. It is obvious that the fourth-order diffusion smear the sharp roll up of the vortex sheet and suppresses the nonlinearity.

iv) Simulation in linear region

Simulation in the linear region can be done in the same condition as chapter 4. Comparison between the computational results obtained by Kawamura's method and

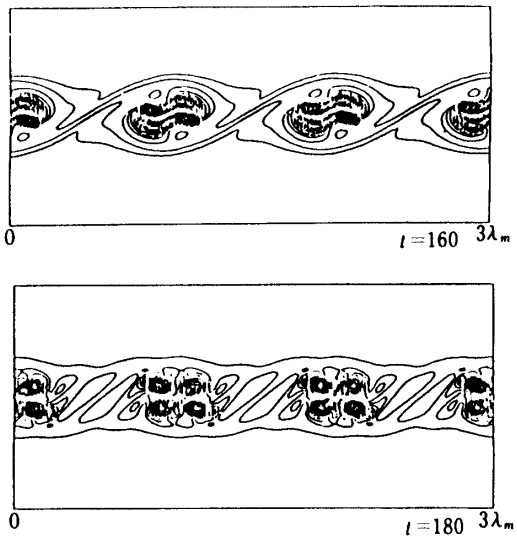

Fig. 16. Temporal evolution of the vorticity contours obtained by Kawamura's method with step 0.04 from t=160 to 180 (continued).
(monochronic initial disturbance and cyclic boundary condition are adopted)

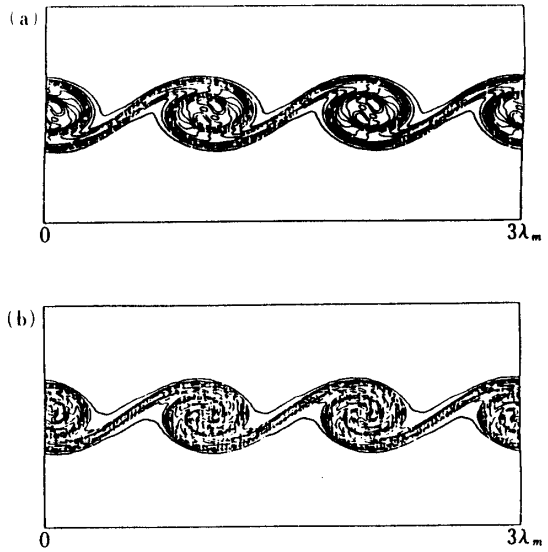

Fig. 17. Vorticity contours with step 0.04.
(a) Conventional Kawamura's method.
(b) Kawamura's method with 6th-8th diffusion in place of 4th diffusion.
(monochronic initial disturbance and cyclic boundary condition are adopted)

results obtained by the linear theory of Michalke [29], seems to be quite good in the sense of both growth rate and the contour pattern of vorticity. However, it must be noted that the growth rate obtained by Kawamura's one is larger by 5% than the linear theory (see Fig. 8).

v) Simulation in nonlinear regime in two grid system; fine one and coarse one

If the flow phenomena in the nonlinear regime, where strong roll up due to vortices occurs, are simulated by Kawamura's method using a fine grid system (about 22 points par wave length), in the same way as mentioned in chapter 4, the strong vorticity region that has no physical meaning takes place, thus resulting in violation of the simulation (see Fig. 16). The reason for this is in that the Kawamura's method does not simulates two cascade processes, indicating that it may be inadequate to predict the strong nonlinear phenomena accurately.

If a coarse grid system (about 8 points par wave length) is used to simulate the same phenomena as mentioned above, there appears no such strong vortex roll up, because the grid system can not resolve them (see Fig. 3). Therefore, the results obtained in the early stage of the simulation seems to be very reasonable because of nonexistence of the physically unreasonable vorticity. However, the present results indicate a trend to lose gradually its regularity, and vortex sheet will be deformed finally, whereas the simulation by the present method still preserves its regular vortex sheet (see Fig. 2). This clearly indicates that Kawamura's method does not have error isotropy, so that the accumulation of non-isotropic error distorts vortex sheet.

References

[1] Grinstein, F. F., Oran, E. S., and Boris, J. P., "Numerical Simulations of asymmetric Mixing in Planar shear Flows," NRL Memorandum Report 5621, August 23, 1985.

[2] Fujiwara, T., Taki, S., and Arashi, K., "Numerical Analysis of a Reacting Flow in H_2/O_2 Rocket Combustor Part 1: Analysis of Turbulent Shear flow," AIAA Paper 86-0528.

[3] Arakawa, A., "Computational Design for Long-Term Numerical Integration of the Equations of Fluid Motion: Two-Dimensional Incompressible Flow. Part I," *Journal of Computational Physics*, Vol. 1, 1966, pp. 119-143.

[4] Platzman, G. W., *J. Meteorol*, Vol. 18, 1961, pp. 31-37.

[5] Orszag, S. A., "Numerical simulation of incompressible flows within simple boundaries. I. Galerkin (spectral) representations," *Studies in Appl. Math.*, Vol. 50, 1971, pp. 293-327.

[6] Satofuka, N., Symp. on Applied Mathematics and Information sciences, Kyoto University, Kyoto, March, 29-31, 1981.

[7] Abe, T., "Coherent Structure Formation by Inverse Cascade Process in Turbulent Mixing Layer," ISAS Research Note, ISAS RN 227.

[8] Fjørtoft, R., "On the Changes in the Spectral Distribution of Kinetic energy for Two-dimensional, Nondivergent Flow," *Tellus*, Vol. 5, 1953, pp. 225-230.

[9] Kraichnan, R. H., "Inertial-range transfer in two- and three-dimensional turbulence," *Journal of Fluid Mech.*, Vol. 47, 1971, pp. 525-535.

[10] Herring, J. R., Orszag, S. A., Kraichnan, R. H. and Fox, D. G., "Decay of two-dimensional homogeneous turbulence," *Journal of Fluid Mech.*, Vol. 66, 1974, pp. 417-444.

[11] Fornberg, B., "On a Fourier method for the integration of hyperbolic equations," *SIAM J. Numer. Anal.*, Vol. 11, 1975, pp. 509-528.

[12] Kreiss, H. O. and Oliger, J., "Comparison of accurate methods for the integration of hyperbolic equations," *Tellus*, Vol. 24, 1972, pp. 192-215.

[13] Fornberg, B., "A Numerical Study of 2-D turbulence," *Journal of Computational Physics*, Vol. 25, 1977. pp. 1-31.

[14] Lilly, D. K., "Numerical simulation of developing and decaying two-dimensional turbulence," *Journal of Fluid Mech.*, Vol. 45, 1971, pp. 395-415.

[15] Michalke, A., "On spatially growing disturbances in an inviscid shear layer," *Journal of Fluid Mech.*, Vol. 23, 1965, pp. 521-544.

[16] Kransny, R., "Desingularization of Periodic Vortex Sheet roll-up," *Journal of Computational*

Vol. 65, 1986, pp. 292–313.

[17] Freymuth, P., "On transition in a separated laminar boundary layer," *Journal of Fluid Mech.*, Vol. 25, 1966, pp. 683–704.

[18] Kawamura, T., "Numerical Study of High Reynolds Number Flow around a Circular Cylinder," Dr. Thesis of University Tokyo, October 1983.